
DEEP PROJECTION NETWORKS FOR LEARNING TIME-HOMOGENEOUS DYNAMICAL SYSTEMS

A PREPRINT

Vladimir R. Kostic*
Istituto Italiano di Tecnologia
University of Novi Sad
vladimir.kostic@iit.it

Pietro Novelli *
Istituto Italiano di Tecnologia
pietro.novelli@iit.it

Riccardo Grazzi
Istituto Italiano di Tecnologia
riccardo.grazzi@iit.it

Karim Lounici
CMAP École Polytechnique
karim.lounici@polytechnique.edu

Massimiliano Pontil
Istituto Italiano di Tecnologia
University College London
massimiliano.pontil@iit.it

July 20, 2023

ABSTRACT

We consider the general class of time-homogeneous dynamical systems, both discrete and continuous, and study the problem of learning a meaningful representation of the state from observed data. This is instrumental for the task of learning a forward transfer operator of the system, that in turn can be used for forecasting future states or observables. The representation, typically parametrized via a neural network, is associated with a projection operator and is learned by optimizing an objective function akin to that of canonical correlation analysis (CCA). However, unlike CCA, our objective avoids matrix inversions and therefore is generally more stable and applicable to challenging scenarios. Our objective is a tight relaxation of CCA and we further enhance it by proposing two regularization schemes, one encouraging the orthogonality of the components of the representation while the other exploiting Chapman-Kolmogorov's equation. We apply our method to challenging discrete dynamical systems, discussing improvements over previous methods, as well as to continuous dynamical systems.

1 Introduction

Dynamical systems are mathematical models that describe the evolution of state variables over time. These models, often represented by nonlinear differential equations (ordinary or partial) and possibly stochastic, have wide-ranging applications in science and engineering. They find utility in various fields such as climate sciences [10, 14], finance [41], atomistic simulations [36, 37, 46], and open quantum system dynamics [19, 32], among others.

In recent years, the abundance of emerging machine learning algorithms has sparked a growing interest on data-driven dynamical systems. Two powerful paradigms have emerged: deep neural networks (DNN) and kernel based. The latter are backed up by solid statistical guarantees [1, 12, 25, 26], and leverage the concept of reproducing kernel Hilbert spaces (RKHS) to map the input data into a feature space, where linearly parameterized models can be learned efficiently. However, in complex dynamical systems selecting an appropriate kernel function may be a hard task, requiring a significant amount of experimentation and expertise. The former on the other hand, are very effective in learning complex data representations [18], and benefit from a solid ecosystem of software and tools making the learning process feasible on large scale systems. Their statistical analysis, however, is still in its infancy with only few results available on their generalization properties.

*Equal contribution, corresponding authors.

Kernel-based methods hinge on the powerful idea of learning dynamical systems by lifting their definition over a space of functions and then studying the associated *transfer operator*. Transfer operators capture the average evolution of functions of the state (observables) over time. These operators are *linear* and under additional assumptions admit a spectral decomposition, which provides an interpretable tool to analyse and control the behaviour of non-linear systems, see e.g. [9, 28] and references therein, where, for deterministic dynamical systems, they are also known as Koopman operators. The usefulness of the transfer operator approach critically relies on the appropriate choice of their domain of definition. In particular, in order to benefit from the spectral decomposition, one needs to find a linear space of functions \mathcal{F} that is *invariant* under the action of the transfer operator. In kernel-based methods such a space is implicitly associated to the kernel function, and the previous sentence provides mathematical meaning to the problem of choosing a “good” kernel. Unfortunately, the analytical form of transfer operators is often intractable or unavailable, especially in complex or poorly understood systems, posing challenges in constructing invariant representations.

In this paper we build upon both kernel and DNN paradigms trying to grasp the best of both worlds. Our objective is to use DNNs to identify a finite dimensional feature space in which the dynamics is accurately represented. We may then forward the learned feature map to kernel-based algorithms for the actual operator regression task. Our method is agnostic to the choice of neural network architecture and is robust under changes of the training hyperparameters. Furthermore, the approach benefits from a differentiable score functional, enhancing the stability of the training process. Finally, it can be applied to both discrete and continuous systems, leveraging the time-homogeneous property of the transfer operator through the Chapman-Kolmogorov equation to facilitate learning.

Previous work. Extensive research has been conducted on learning dynamical systems from data. The monographs [9, 28] are standard references in this field. To learn Koopman operators we mention the works [1, 8, 12, 24–26, 53] presenting kernel-based algorithms, and [7, 13, 34] based on deep learning schemes. Obtaining meaningful representations of the state of the system to be used in conjunction with Koopman operator learning is a critical challenge, tackled by many authors. We mention the collection of works [6, 34, 40, 52], where a representation is learned via encoding-decoding schemes, as well as the papers [24, 30, 35, 36, 48, 54, 55] addressing the problem of learning invariant subspaces of the Koopman operator. Mostly related to our contributions are the work [3], which introduced deep canonical correlation analysis and especially VAMPnets [36, 54], which extended this approach to learn transfer operators. Their objective functional, however, is based on the inversion of empirical covariance matrices of the learned features, which may be numerically unstable and causes significant issues during training on large scale problems. Moreover, theoretical results in [54] at the basis of the DNN approach in [36], are limited to Hilbert-Schmidt transfer operators, whereas we require only compactness. Hence, notably, our approach is sound for stochastic dynamical systems without additional constraints of having square integrable transition density [29].

Contributions. Our main contributions are summarized as follows: **1)** We present a general framework, which we name deep projection networks (DPNets), for learning a latent representation of the state of a dynamical system. This representation based on orthogonal projections in data-spaces is designed to span a principal invariant space of the associated transfer operator, and can be learned for both discrete and continuous dynamical systems; **2)** The representations are learned by optimizing a differentiable objective function. We interpret the objective as a tight relaxation of canonical correlation analysis’s objective that has been used alongside DNN in previous works; **3)** We introduce two regularization schemes to be coupled to the objective function. The first one is designed to have mutually decorrelated feature components, while the second exploits the time-homogeneity of the system to facilitate learning; **4)** We present extensive numerical experiments testing our framework in a variety of settings, showing its generality, the importance of the relaxation and regularization, and its competitive performance.

Notation. We let \mathbb{N} the set of natural numbers and $\mathbb{N}_0 = \{0\} \cup \mathbb{N}$. For $m \in \mathbb{N}$ we denote $[m] := \{1, \dots, m\}$. If \mathcal{T} is a compact linear operator on two Hilbert spaces we let $\sigma_i(\mathcal{T})$ be its i -th largest singular value, we let $(\mathcal{T})^\dagger$ be the Moore-Penrose pseudo-inverse, and \mathcal{T}^* the adjoint operator. Finally we denote by $\|\cdot\|$ the spectral norm (largest singular value) of a matrix or compact operator, and by $\|\cdot\|_{\text{HS}}$ the Hilbert-Schmidt norm of an operator (Frobenius norm of a matrix).

2 Problem and approach

Let $(X_t)_{t \in \mathbb{T}} \subseteq \mathcal{X}$ be a stochastic process in some state space \mathcal{X} , where the time index t can either be discrete ($\mathbb{T} = \mathbb{N}_0$) or continuous ($\mathbb{T} = [0, +\infty)$). For every pair of time steps $t, t' \in \mathbb{T}$, with $t' \geq t$, the *forward transfer operator* $\mathcal{T}_{t,t'}$ evolves an observable $f : \mathcal{X} \rightarrow \mathbb{R}$, from time $t \in \mathbb{T}$ to time t' , by the conditional expectation

$$\mathcal{T}_{t,t'}(f) := \mathbb{E}[f(X_{t'}) | X_t = \cdot]. \quad (1)$$

For a large class of (stochastic) dynamical systems, these *linear* operators are *time-homogeneous*, i.e. they only depend on the time-step $\Delta t = t' - t$, hence we write $\mathcal{T}_{t,t'} = \mathcal{T}_{\Delta t}$.

Forward transfer operators can be studied on various domains of definition \mathcal{F} , understood as spaces of observables. When \mathcal{F} is invariant under the action of \mathcal{T}_Δ , that is $\mathcal{T}_{\Delta t}[\mathcal{F}] \subseteq \mathcal{F}$, and the dynamics is deterministic, they are also known as Koopman operators. Common choices for \mathcal{F} are the space of bounded continuous functions and the space of square integrable functions with respect to the invariant distribution, when one exists, which we will study in Sec. 5.

The principal objective of this work is to *learn an invariant space \mathcal{F} from observations of the dynamical system*, and then use it, on seen or unseen data, to approximate the corresponding transfer operator. In order to introduce the learning problem, we use transfer operators defined on the spaces determined by the evolving state distributions, from which data will be sampled. Let X and X' be two \mathcal{X} -valued random variables with probability measures μ and μ' , respectively, where X is the initial state of the system and X' is the state after Δt time. Then the transfer operator can be defined as $\mathcal{T}_{\Delta t}: L^2_\mu(\mathcal{X}) \rightarrow L^2_{\mu'}(\mathcal{X})$. To ease the presentation, and without the loss of generality, in what follows we discuss the case $\Delta t = 1$ and use the shorthand notation $\mathcal{T} := \mathcal{T}_1$.

Our approach is based on the following algebraic reasoning. If \mathcal{H} is a closed subspace of both $L^2_\mu(\mathcal{X})$ and $L^2_{\mu'}(\mathcal{X})$, then it is an invariant subspace of the transfer operator \mathcal{T} , i.e. $\mathcal{T}[\mathcal{H}] \subseteq \mathcal{H}$, if and only if

$$[I - P_{\mathcal{H}}]\mathcal{T}P'_{\mathcal{H}} = 0, \quad (2)$$

where I is identity operator on \mathcal{H} , $P_{\mathcal{H}}$ and $P'_{\mathcal{H}}$ are orthogonal projections onto \mathcal{H} in $L^2_\mu(\mathcal{X})$ and $L^2_{\mu'}(\mathcal{X})$, respectively. Classical numerical algorithms for spectral computation developed to approximate invariant subspaces (see e.g. [17]) aim to minimize the norm of the operator in the l.h.s. of (2). Unfortunately, they are unfeasible in our setting, since we do not have access to \mathcal{T} .

To overcome the above problem, we take a different route that uses the singular value decomposition of \mathcal{T} , which exists when \mathcal{T} is a compact operator². Indeed, if \mathcal{H} and \mathcal{H}' are spanned respectively by the leading r left and right singular functions of \mathcal{T} , then $P_{\mathcal{H}}\mathcal{T}$ is the r -truncated SVD of \mathcal{T} , i.e. its best rank- r approximation [16]. Consequently, one has that $\|[I - P_{\mathcal{H}}]\mathcal{T}P'_{\mathcal{H}'}\| = 0$, where $P'_{\mathcal{H}'}$ is the orthogonal projection onto \mathcal{H}' in $L^2_{\mu'}(\mathcal{X})$. Moreover, when the same space \mathcal{H} is used in computing the projections, we have that

$$0 \leq \|[I - P_{\mathcal{H}}]\mathcal{T}P'_{\mathcal{H}}\| \leq \|[I - P_{\mathcal{H}}]\mathcal{T}\| \leq \sigma_{r+1}(\mathcal{T}). \quad (3)$$

Thus, if the problem is "easy", e.g. \mathcal{T} is of rank at most r , then the lower bound in (3) is attained and \mathcal{H} is the leading invariant subspace of \mathcal{T} . Otherwise, if the problem is "hard", then \mathcal{H} is only approximately the leading invariant subspace. However even in the worst case, by rising r we can achieve an arbitrarily good approximation. Finally, the lower bound in (3) can sometimes be obtained regardless of the value of r and only with one projection, as we elaborate in Sec. 5.

The above argument reduces the task of computing an invariant or approximately invariant r -dimensional subspace to computing the r -truncated SVD of \mathcal{T} . To this end, we rely on the application of Eckart-Young-Mirsky's Theorem (Lem. 1 in App. B) to conclude that when

$$\max \left\{ \|P_{\mathcal{H}}\mathcal{T}P'_{\mathcal{H}'}\|_{\text{HS}}^2 \mid \dim(\mathcal{H}) \leq r, \dim(\mathcal{H}') \leq r \right\} \quad (4)$$

is achieved, \mathcal{H} and \mathcal{H}' are spanned by the leading r left and right singular vectors of \mathcal{T} , respectively. To perform such maximization, we choose two families of feature maps

$$\psi_w(x) := (\psi_{w,1}(x), \dots, \psi_{w,r}(x)) \in \mathbb{R}^r, \text{ and } \psi'_w(x) := (\psi'_{w,1}(x), \dots, \psi'_{w,r}(x)) \in \mathbb{R}^r, \quad (5)$$

parameterized by a parameter w taking values in some set \mathcal{W} . We also introduce the corresponding function spaces

$$\mathcal{H}_w := \text{span}(\psi_{w,j})_{j \in [r]}, \quad \text{and} \quad \mathcal{H}'_w := \text{span}(\psi'_{w,j})_{j \in [r]}. \quad (6)$$

Then, after some algebra (see Lem. 2 in App. B) the objective can be expressed using the (uncentered) covariance and cross-covariance matrices in the feature spaces,

$$\mathcal{P}(w) = \|P_{\mathcal{H}_w}\mathcal{T}P'_{\mathcal{H}'_w}\|_{\text{HS}}^2 = \|(C_X^w)^{\dagger/2}C_{XX'}^w(C_{X'}^w)^{\dagger/2}\|_{\text{HS}}^2, \quad (7)$$

where

$$C_X^w := \mathbb{E} \psi_w(X)\psi_w(X)^\top, \quad C_{X'}^w := \mathbb{E} \psi'_w(X')\psi'_w(X')^\top \quad \text{and} \quad C_{XX'}^w := \mathbb{E} \psi_w(X)\psi'_w(X')^\top. \quad (8)$$

The objective in (7) indicates the potential to estimate w from data by substituting the true covariances with empirical ones, a topic we address next.

²This property is fulfilled by a large class of Markov processes (see e.g. [26]) and is much weaker than requiring the operator be Hilbert-Schmidt as in [36].

3 Deep projections score functional

We now present our approach to optimize the score functional $\mathcal{P}: \mathcal{W} \rightarrow [0, +\infty)$ derived in (7). Since in the following we parameterize the feature maps with different DNNs, we name our approach *Deep-Projection-Networks* (DPNets). Note first that if C_X^w and $C_{X'}^w$ are nonsingular, the score reduces to $\|(C_X^w)^{-\frac{1}{2}} C_{XX'}^w (C_{X'}^w)^{-\frac{1}{2}}\|_{\text{F}}^2$ which is the objective of canonical correlation analysis (CCA) [21, 22] in feature space. By maximizing this score, therefore, we look for the strongest *linear correlation* between \mathcal{H}_w and \mathcal{H}'_w . When DNNs are used to parametrize the feature maps (5), maximizing the score \mathcal{P} aligns with the objective of Deep-CCA [3], also employed in [36] in the context of molecular kinetics.

However, the covariances C_X^w and $C_{X'}^w$ are in general non-invertible, making the score \mathcal{P} non-differentiable. Indeed, unless the rank of both covariances is stable for every $w \in \mathcal{W}$ [16], we might have exploding gradients. Even ignoring differentiability issues, the use of the pseudo-inverse, as well as the use of the inverse in the non-singular case, can introduce severe numerical instabilities when evaluating \mathcal{P} and its gradients during the training process. More precisely, the numerical conditioning of evaluating \mathcal{P} using (7) scales with $\lambda_1(C_X^w)/\lambda_{\min}^+(C_X^w)$, which can be very large in practical situations (see e.g. the fluid dynamics example in Sec. 6). To overcome this issue, we introduce the relaxed score

$$\mathcal{S}(w) := \frac{\|C_{XX'}^w\|_{\text{HS}}^2}{\|C_X^w\| \|C_{X'}^w\|} \leq \mathcal{P}(w). \quad (9)$$

A key advantage of this approach is that the score \mathcal{S} is both differentiable (apart from the trivial case $C_X^w, C_{X'}^w = 0$) and has stable gradients, since we avoid matrix inversion. Indeed, computing \mathcal{S} is always well-conditioned, since the conditioning of $\lambda_1(C_X^w)$ equals one, as C_X^w is always self-adjoint.

We now introduce a regularization scheme which can be used to accelerate the learning of an invariant subspace for \mathcal{T} . Since for all $i, j \in [r]$ we have that $\langle \psi_{w,i}, \psi_{w,j} \rangle_{L_\mu^2(\mathcal{X})} = (C_X^w)_{i,j}$, it is clear that when $C_X^w = I$, the functions $\psi_{w,i}$ form an orthonormal set, and the covariance C_X^w is optimally conditioned. We therefore propose a (spectral) matrix regularizer $\mathcal{R}: \mathbb{R}^{r \times r} \rightarrow \mathbb{R}_+$ that is zero if and only if it is applied to the identity matrix. Clearly, while the maximization of either \mathcal{P} or \mathcal{S} correlates \mathcal{H}_w and \mathcal{H}'_w , the role of \mathcal{R} is to *decorrelate* the features within each space guiding the maximization towards the optimum. Two natural choices are $\mathcal{R}(C) := \frac{1}{2} \|I - C\|_{\text{HS}}^2$ or $\mathcal{R}(C) := r + \text{tr}[C \log(C) - C]$. This leads us to consider regularized scores

$$\mathcal{P}^\gamma(w) = \mathcal{P}(w) - \gamma (\mathcal{R}(C_X^w) + \mathcal{R}(C_{X'}^w)), \quad \mathcal{S}^\gamma(w) = \mathcal{S}(w) - \gamma (\mathcal{R}(C_X^w) + \mathcal{R}(C_{X'}^w)). \quad (10)$$

The following theorem is the theoretical backbone of our approach.

Theorem 1. *Let $\mathcal{T}: L_\mu^2(\mathcal{X}) \rightarrow L_\mu^2(\mathcal{X})$ be compact. If $\mathcal{H}_w \subseteq L_\mu^2(\mathcal{X})$ and $\mathcal{H}'_w \subseteq L_{\mu'}^2(\mathcal{X})$, then for all $\gamma \geq 0$*

$$\mathcal{S}^\gamma(w) \leq \mathcal{P}^\gamma(w) \leq \sigma_1^2(\mathcal{T}) + \dots + \sigma_r^2(\mathcal{T}). \quad (11)$$

Moreover, if $(\psi_{w,j})_{j \in [r]}$ and $(\psi'_{w,j})_{j \in [r]}$ are leading r left and right singular functions of \mathcal{T} , respectively, then both equalities in (11) hold. Finally, if the operator \mathcal{T} is Hilbert-Schmidt, $\sigma_r(\mathcal{T}) > \sigma_{r+1}(\mathcal{T})$ and $\gamma > 0$, then the “only if” relation is satisfied up to unitary equivalence.

As the previous result shows, under generic assumptions, both the regularized score and its relaxation achieve the global maximum if and only if the embeddings $\psi_{w,1}, \dots, \psi_{w,r}$ and $\psi'_{w,1}, \dots, \psi'_{w,r}$ essentially coincide with the leading r left and right singular functions of \mathcal{T} , respectively. Moreover, due to (3) whenever $\sigma_{r+1}(\mathcal{T})$ is small enough we also have that $\psi_{w,1}, \dots, \psi_{w,r}$ span a space which is approximately invariant under the action of \mathcal{T} . The dictionaries of optimally learned functions serve us to construct Hilbert spaces \mathcal{H}_w and \mathcal{H}'_w in (6) that can be used for prediction or forecasting on downstream tasks; we discuss this in more details in Sec. 4.

To clarify the importance of orthonormality regularization term \mathcal{R} , we stress that, if no regularization is used ($\gamma = 0$) but \mathcal{T} is Hilbert-Schmidt and $\sigma_r(\mathcal{T}) > \sigma_{r+1}(\mathcal{T})$, then both the score and its relaxation achieve maximum if and only if \mathcal{H}_w and \mathcal{H}'_w are spanned by leading r left and right singular functions of \mathcal{T} , respectively (see Rem. 2 of App. C). This means that without regularization, the learned features $(\psi_{w,j})_{j \in [r]}$ may form an ill-conditioned basis of $\mathcal{H}_w \subseteq L_\mu^2(\mathcal{X})$, i.e. $\lambda_1(C_X^w)/\lambda_r(C_X^w) \gg 1$, which leads to ill-conditioned estimation of the spectral decomposition of the transfer operator via RKHS \mathcal{H}_w due to large metric distortions, see [26]. This is illustrated in Pendulum experiment in Sec. 6.

Learning from multiple time-steps Finally we discuss how the time-homogeneous property of the transfer operator can be used to facilitate learning across multiple time steps. For simplicity of presentation, we only discuss the case when we have three (possibly not equally spaced) observations of the process, X , X' and X'' , where X' is the evolution of X after time Δt and X'' is the evolution after the additional $\Delta t'$. We now have additional spaces

$\mathcal{H}_w'' := \text{span}(\psi_{w,j}'')_{j \in [r]} \subseteq L^2_{\mu''}(\mathcal{X})$, where $X'' \sim \mu''$, a projection $P_{\mathcal{H}_w''}''$ in $L^2_{\mu''}(\mathcal{X})$ and three different transfer operators to consider $\mathcal{T}_{\Delta t}: L^2_{\mu'}(\mathcal{X}) \rightarrow L^2_{\mu}(\mathcal{X})$, $\mathcal{T}_{\Delta t'}: L^2_{\mu''}(\mathcal{X}) \rightarrow L^2_{\mu'}(\mathcal{X})$ and $\mathcal{T}_{\Delta t+\Delta t'}: L^2_{\mu''}(\mathcal{X}) \rightarrow L^2_{\mu}(\mathcal{X})$. While different, they are intimately related since they are transfer operators of the *same time-homogeneous process*. A formal means of relating them is through the Chapman-Kolmogorov equation [2], which connects the joint probability distribution of a stochastic process at different times to the conditional probability distribution of the process at an intermediate time. Namely, we have that

$$\mathcal{T}_{\Delta t+\Delta t'} = \mathcal{T}_{\Delta t} \mathcal{T}_{\Delta t'}. \quad (12)$$

We can leverage this equation to jointly learn all three transfer operators, or in our context, learn the feature maps ψ_w , ψ'_w and ψ''_w as follows. If the pairs (ψ_w, ψ'_w) , (ψ'_w, ψ''_w) and (ψ_w, ψ''_w) all satisfy the optimality conditions of Thm. 1 for $\gamma > 0$, then the corresponding cross-covariance represent the action of the transfer operators on the feature spaces. Specifically, since in this case $P_{\mathcal{H}_w} \mathcal{T}_{\Delta t} P_{\mathcal{H}'_w} = P_{\mathcal{H}_w} \mathcal{T}_{\Delta t}$ is just r -truncated SVD of $\mathcal{T}_{\Delta t}$, Chapman-Kolmogorov equation implies

$$\mathcal{K}_{\Delta t, \Delta t'}(w) := \|C_{XX'}^w C_{X'X''}^w - C_{XX''}^w\| = \|P_{\mathcal{H}_w} \mathcal{T}_{\Delta t} P_{\mathcal{H}'_w} \mathcal{T}_{\Delta t'} P_{\mathcal{H}_w''} - P_{\mathcal{H}_w} \mathcal{T}_{\Delta t+\Delta t'} P_{\mathcal{H}_w''}\| = 0.$$

Using the norm above, we can train DPNets for multiple time-steps via the doubly regularized score

$$\mathcal{S}_{\Delta t, \Delta t'}^{\gamma, \eta}(w) = \frac{1}{2} (\mathcal{S}_{\Delta t}^{\gamma}(w) + \mathcal{S}_{\Delta t'}^{\gamma}(w)) - \eta \mathcal{K}_{\Delta t, \Delta t'}(w), \quad (13)$$

which is illustrated in Fluid Dynamics experiment in Sec. 6.

4 Methods

In this section, we address the practical training of DPNets to learn the representations ψ_w and ψ'_w . We then demonstrate the application of these learned representations in downstream tasks, such as next state prediction or spectral decomposition approximation. We keep the presentation brief and defer a detailed discussion to App. D.

Learning the feature map As suggested above, to derive practical methods, one needs to replace (population) covariances and cross-covariance with their empirical counterparts. In practice, when we aim to learn the transfer operator from the space of X to that of X' , we start from a dataset $\mathcal{D} = (x_i, x'_i)_{i \in [n]}$ consisting of samples from the joint distribution of (X, X') . Recalling that marginals μ and μ' of X and X' are in general different, we train a DNN by minimizing the empirical score functionals $\widehat{\mathcal{P}}_n^{\gamma}: \mathcal{W} \rightarrow \mathbb{R}$ and $\widehat{\mathcal{S}}_n^{\gamma}: \mathcal{W} \rightarrow \mathbb{R}$ obtained from $\mathcal{P}^{\gamma}: \mathcal{W} \rightarrow \mathbb{R}$ and $\mathcal{S}^{\gamma}: \mathcal{W} \rightarrow \mathbb{R}$, respectively, by replacing C_X^w , $C_{X'}^w$, and $C_{XX'}^w$ with their empirical counterparts

$$\widehat{C}_X^w := \frac{1}{n} \sum_{i \in [n]} \psi_w(x_i) \psi_w(x_i)^\top, \quad \widehat{C}_{X'}^w := \frac{1}{n} \sum_{i \in [n]} \psi'_w(x'_i) \psi'_w(x'_i)^\top \quad (14)$$

and

$$\widehat{C}_{XX'}^w := \frac{1}{n} \sum_{i \in [n]} \psi_w(x_i) \psi'_w(x'_i)^\top. \quad (15)$$

In App. D we derive theoretical guarantees for the concentration of our empirical score $\widehat{\mathcal{S}}_n^{\gamma}$ to the true score \mathcal{S}^{γ} for any fixed w . Obtaining uniform guarantees over w requires advanced tools from the theory of empirical process and regularity assumptions on the representations.

Operator regression and prediction We next discuss how to design an estimator of the transfer operator between the learned subspaces, $\widehat{\mathcal{T}}_w: \mathcal{H}'_w \rightarrow \mathcal{H}_w$, that we can use, given a initial state $x \in \mathcal{X}$ to predict the average evolution $\mathbb{E}[f(X') | X = x]$ of an observable $f \in L^2_{\mu'}(\mathcal{X})$. When $\|f\| \leq 1$ a standard decomposition gives that

$$\|\mathcal{T}f - \widehat{\mathcal{T}}_w P_{\mathcal{H}'_w} f\| \leq \|\mathcal{T}[I - P_{\mathcal{H}'_w}]\| + \|[I - P_{\mathcal{H}_w}] \mathcal{T} P_{\mathcal{H}'_w}\| + \|P_{\mathcal{H}_w} \mathcal{T} P_{\mathcal{H}'_w} - \widehat{\mathcal{T}}_w\|. \quad (16)$$

Using Thm. 1, if w is optimal, the first term in the r.h.s. of (16) is bounded by $\sigma_{r+1}(\mathcal{T})$ and the second is zero. The last term is the operator norm error $\|P_{\mathcal{H}_w} \mathcal{T} P_{\mathcal{H}'_w} - \widehat{\mathcal{T}}_w\|$ which can be tightly bounded [26]. This observation indicate that our approach will work well if r is large enough and we have collected enough data on the downstream task.

Following the reasoning in [26] one sees that every estimator is of the form $\widehat{\mathcal{T}}_w = E_w \widehat{T}(E'_w)^*$, where $\widehat{T} \in \mathbb{R}^{r \times r}$, the operator $E_w: \mathbb{R}^r \mapsto \mathcal{H}_w$ is such that $E_w v = \psi_w(\cdot)^\top v$, the operator $E'_w: \mathbb{R}^r \mapsto \mathcal{H}'_w$ is defined similarly from ψ'_w , and $(E'_w)^*$ is its adjoint. Different estimators of matrix \widehat{T} can be computed from data $(x_i, x'_i)_{i \in [n]}$ (either seen or unseen during training time). A natural one is the least square (LS) estimator $\widehat{T} := (\widehat{C}_X^w)^\dagger \widehat{C}_{XX'}^w$.

Once the regression is performed, recalling that X' is a $\Delta t = 1$ step ahead evolution of X we can use it to approximate $\mathbb{E}[f(X') | X = x] \approx (\widehat{\mathcal{T}}_w f)(x)$ for $f: \mathcal{X} \rightarrow \mathbb{R}$.

Estimating the spectral decomposition and forecasting Another downstream task is to estimate eigenvalues and eigenfunctions of the transfer operator. This is meaningful only if the operator is an endomorphism, i.e. it maps the space into itself. In this case, after training DPNet we will use just one representation ψ_w and its r -dimensional space of functions $\mathcal{H}_w := \text{span}(\psi_{w,j})_{j \in [r]}$ to perform the operator regression as above, obtaining an estimator $\widehat{\mathcal{T}}_w = E_w \widehat{T} E_w^* : \mathcal{H}_w \rightarrow \mathcal{H}_w$, for some matrix $\widehat{T} \in \mathbb{R}^{r \times r}$. The spectral decomposition of the operator $\widehat{\mathcal{T}}_w$ can be computed via the spectral decomposition of the matrix \widehat{T} . Indeed if $(\widehat{\lambda}_i, \widehat{u}_i, \widehat{v}_i) \in \mathbb{C} \times \mathbb{C}^d \times \mathbb{C}^d$ is an eigen-triplet made of eigenvalue, left eigenvector and right eigenvector, that is $\widehat{T}\widehat{v}_i = \widehat{\lambda}_i \widehat{v}_i$, $\widehat{u}_i^* \widehat{T} = \widehat{\lambda}_i \widehat{u}_i^*$ and $\widehat{u}_i^* \widehat{v}_k = \delta_{i,k}$, $i, k \in [r]$, we directly obtain that $E_w \widehat{u}_i$ and $E_w \widehat{v}_i$ are i -th left and right eigenfunctions of $\widehat{\mathcal{T}}_w$, respectively. Thus, we have the spectral decomposition

$$\widehat{\mathcal{T}}_w = \sum_{i \in [r]} \widehat{\lambda}_i \widehat{g}_i \otimes \widehat{f}_i, \quad \text{where} \quad \widehat{g}_i(x) := \psi_w(x)^\top \widehat{v}_i \quad \text{and} \quad \widehat{f}_i(x) := (\widehat{u}_i)^* \psi_w(x). \quad (17)$$

If the optimum is computed during training, we have that $\|[I - P_{\mathcal{H}_w}] \mathcal{T} P_{\mathcal{H}_w}'\| \leq \varepsilon$, where, with high probability, depending of the number of samples, the size of the representation space r and the optimization procedure, ε is small. Hence, using (16), we obtain the eigenvalue-eigenfunction approximation error

$$\|\mathcal{T} \widehat{g}_i - \widehat{\lambda}_i \widehat{g}_i\| \leq \varepsilon \|\widehat{g}_i\|.$$

Finally, since the dynamics is approximated by the spectral decomposition, we can use it to efficiently forecast for several time-steps in the future using what is known as extended dynamic mode decomposition (EDMD) [9].

5 Stationary Markov processes

In this section we focus on stationary processes. We assume that the process $(X_t)_{t \in \mathbb{T}}$ admits an *invariant (stationary) distribution* π , that is if $X_t \in L^2_\pi(\mathcal{X})$ then also $X_{t'} \in L^2(\mathcal{X})$ for every $t' \in \mathbb{T}$, $t' \geq t$; see [43]. In this setting, Chapman-Kolmogorov equation (12) implies that $\mathcal{T}_{\Delta t} = \mathcal{T}^{\Delta t}$, for all Δt . Hence, if the operator \mathcal{T} is normal, meaning that $\mathcal{T}\mathcal{T}^* = \mathcal{T}^*\mathcal{T}$, then both its left and right singular spaces coincide with the eigenspace of $\mathcal{T}^{\Delta t}$ for each time step Δt . Note that eigenvalues of $\mathcal{T}_{\Delta t}$ depend on Δt , while eigenfunctions do not. An important class of stationary processes with normal transfer operators are *time-reversal invariant* processes, for which \mathcal{T} is self-adjoint, i.e. $\mathcal{T} = \mathcal{T}^*$. This includes the important case of Langevin dynamics, where the spectral decomposition of the transfer operators $\mathcal{T}_{\Delta t}$ is of paramount importance in the study of long-term dynamics and so-called *meta-stable* states of molecular systems [see, e.g., 51].

As noted above, the setting of stationary Markov chains with normal transfer operators allows one to further improve learning. Namely, projections $P_{\mathcal{H}_w}$ and $P_{\mathcal{H}_w}'$ aim to learn the same subspace. Thus, without loss of generality, we can simplify the architecture considering only one embedding ψ_w and obtain in Eq. (3) at the optimum $\|[I - P_{\mathcal{H}_w}] \mathcal{T}_{\Delta t} P_{\mathcal{H}_w}\| = 0$.

The setting of stationary processes allows us to apply deep projection framework also to continuous time processes. To that end, we consider a time-homogeneous stochastic differential equation (SDE).

$$dX_t = A(X_t) dt + B(X_t) dW_t, \quad (18)$$

where function A is the drift, function B is the diffusion, and W_t is a Wiener process [4]. Further we assume that SDE (18) has a stationary distribution π from which we sample data, and we assume that the process is time-reversal invariant w.r.t π . Since the time is now continuous, one cannot reduce the study of the process to \mathcal{T}_1 , but instead needs to work with the family $(\mathcal{T}_{\Delta t})_{\Delta t \geq 0}$ that, appealing to Chapman-Kolmogorov equation, forms a semigroup. Hence, we can study the process by working with the infinitesimal generator of this semigroup $\mathcal{L} : L^2_\pi(\mathcal{X}) \rightarrow L^2_\pi(\mathcal{X})$, which is defined as

$$\mathcal{L} = \lim_{\Delta t \rightarrow 0^+} \frac{\mathcal{T}_{\Delta t} - I}{\Delta t}. \quad (19)$$

In general \mathcal{L} is not a compact operator and not even a bounded one. Hence Eckart-Young-Mirsky theorem cannot be used as in Sec. 3. Here, instead, we rely on the fact that $\mathcal{L} = \mathcal{L}^*$ and introduce the score via *partial trace* of \mathcal{L} w.r.t. to the subspace $\mathcal{H}_w := \text{span}(\psi_{w,j})_{j \in [r]} \subseteq L^2_\pi(\mathcal{X})$, i.e.

$$\mathcal{P}_\partial(w) := \text{tr}(P_{\mathcal{H}_w} \mathcal{L} P_{\mathcal{H}_w}) \quad \text{and} \quad \mathcal{P}_\partial^\gamma(w) := \mathcal{P}_\partial(w) - \gamma \mathcal{R}(C_X^w). \quad (20)$$

Now, having in mind (19), the action of \mathcal{L} is related to time derivatives of the process, hence we introduce the continuous version of the cross-covariance as $C_{X\partial}^w = \mathbb{E}[\psi_w(X) d\psi_w(X)^\top]$, in which $d\psi_w(\cdot)$ is defined via Itô formula (see e.g.

Table 1: State forecasting relative error on pendulum. Mean (std) of $\|x_t - \hat{x}_t\|_2 / \|x_t\|_2$ for state x_t and forecast \hat{x}_t on different future time-steps t over 10 training runs (varying only the network initialization) and 30 validation starting points.

$\theta_0 = 2.4$ (non-linear)			$\theta_0 = 0.8$ (almost linear)		
	\mathcal{P}^γ	$\hat{\mathcal{P}}$		\mathcal{P}^γ	$\hat{\mathcal{P}}$
$t = 1$.003 (.002)	.006 (.007)	.006 (.002)	.016 (.015)	.012 (.025)
$t = 500$.007 (.004)	.066 (.111)	.040 (.020)	.022 (.016)	.196 (.329)
$t = 1000$.013 (.007)	.114 (.176)	.079 (.039)	.030 (.019)	.273 (.418)
Aggregate	.007 (.005)	.063 (.119)	.041 (.031)	.022 (.017)	.179 (.325)

[4]) as

$$d\psi_w(X) = \nabla\psi_w(X)^\top dX/dt + \frac{1}{2}(dX/dt)^\top \nabla^2\psi_w(X)(dX/dt) \quad (21)$$

$$= \nabla\psi_w(X)^\top A(X) + \frac{1}{2} \text{tr}(B(X)^\top \nabla^2\psi_w(X)B(X)), \quad (22)$$

where (22) follows from (18). We now obtain the following result whose proof is given in App. E.

Theorem 2. *If $\mathcal{H}_w \subseteq L^2_\pi(\mathcal{X})$ and \mathcal{L} has at least $r + 1$ eigenvalues above its essential spectrum, then*

$$\mathcal{P}_\partial(w) = \text{tr}((C_X^w)^\dagger C_{X\partial}^w) \leq \lambda_1(\mathcal{L}) + \dots + \lambda_r(\mathcal{L}), \quad (23)$$

where $\lambda_1(\mathcal{L}) \geq \lambda_2(\mathcal{L}) \geq \dots$ are eigenvalues of \mathcal{L} . Moreover, if for every $j \in [r]$ function $\psi_{w,j}$ is the eigenfunction of \mathcal{L} corresponding to eigenvalue $\lambda_j(\mathcal{L})$, then equality in (23) holds.

Using the above quantities, we can extend the work presented in previous sections to the continuous setting by replacing C_{XX}^w and \hat{C}_{XX}^w by $C_{X\partial}^w$ and $\hat{C}_{X\partial}^w := \frac{1}{n} \sum_{i \in [n]} \psi_w(x_i) d\psi_w(x_i)^\top$, respectively. When we know the drift and diffusion terms in (18), this estimation can be done using (22) and data $\mathcal{D} = (x_i)_{i \in [n]}$ consisting of (possibly not equally spaced in time) samples from a stationary trajectory. Otherwise, we can use (21) and data $\mathcal{D} = (x_i, \frac{d}{dt}x_i)_{i \in [n]}$ containing time derivatives $\frac{d}{dt}x_i$. If not at our disposal, they can be estimated as $\frac{d}{dt}x_i \approx (x_{i+1} - x_i)/\Delta t_i$, which is, clearly, meaningful when the time-step is small enough. At last, we note that details on the operator regression and the dynamic mode decomposition using generator eigenvalues are presented in App. E.

6 Experiments

In this experimental section we show (i) the advantages that the proposed regularized and/or relaxed score has over the score \mathcal{P} related to Deep CCA [3], (ii) that our method makes it possible to learn the generator operator for continuous stochastic dynamical systems, (iii) that our approach can be competitive against koopman autoencoders on the task of forecasting the state of deterministic systems, and (iv) that our relaxed and regularized objective can be used to train GNNs as feature extractors for a chemical system. Additional details and evaluations are in Appendix F.

Pendulum We consider forecasting on a classical example of deterministic non-linear dynamical system - the pendulum with no friction. We use the same experimental setup of [6] where consistent autoencoder model (CAE) is proposed (using the provided code). In particular, in our methods we implement the feature map using the same encoder architecture with a higher number of parameters and increasing the number of output features from 6 to 21 to account for the lack of a decoder network³. Tab. 1 shows the state forecasting error for our approach, with (\mathcal{P}^γ) and without (\mathcal{P}) orthonormality regularization in the training objective, and CAE. We remark that \mathcal{P}^γ outperforms all other methods when $\theta_0 = 2.4$, while it has worse state prediction error at $t = 1$, but better after $t = 500$ when $\theta_0 = 0.8$. As expected, \mathcal{P} was more unstable during training and does not perform well already after few time-steps. In this simple setting, the relaxed objective \mathcal{S}^γ performed generally worse than \mathcal{P}^γ , since orthonormality regularization was sufficient to have stable training.

Fluid dynamics Understanding fluid flow past a cylinder is a classic challenge in fluid dynamics. In this example, our goal is to learn a meaningful embedding of a Navier-Stokes simulation for the transport of a passive scalar by a 2D fluid flow past a cylinder [42]. Each data snapshot comprises a regular 2D grid that encompasses fluid variables, including velocity, pressure, and scalar field concentration at each grid point. To derive meaningful embeddings ψ_w and ψ'_w , we

³note that our next-step decoder is linear and not learned with the network. See Appendix.

employ convolutional neural networks with a standard architecture featuring three Conv-ReLu-Pooling units followed by two dense layers. The dynamics of this system is non-stationary and non-linear, also known to exhibit non-normal dynamics in the statespace, see [49]. These facts, as well as the high-dimensionality of the inputs (a 100×200 grid with 4 features at each point) makes this example very challenging from a numerical perspective. Despite the direct optimization of \mathcal{P}^γ may offer faster convergence, its vulnerability to numerical instability poses a significant drawback, and we report that we have *never* been able to complete a training loop for ψ_w and ψ'_w while optimizing over \mathcal{P}^γ . The relaxed score, in this situation \mathcal{S}^γ emerges as a compelling choice. The forecasting performance of the models obtained optimizing over \mathcal{S}^γ as in (10) and over $\mathcal{S}^{\gamma,\eta}$ with additional Chapman-Kolmogorov regularization are reported in Fig. 2.

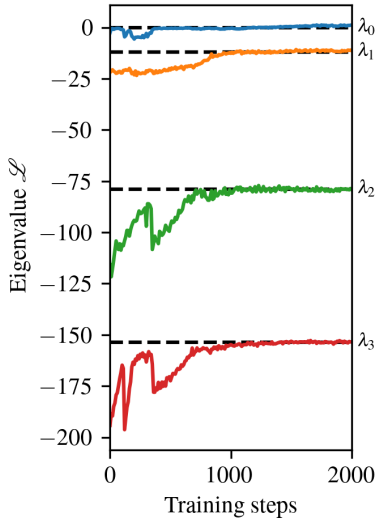


Figure 1: Estimation of the eigenvalues of the generator \mathcal{L} of a SDE using non-evenly sampled validation data during the training of a deep projection embedding.

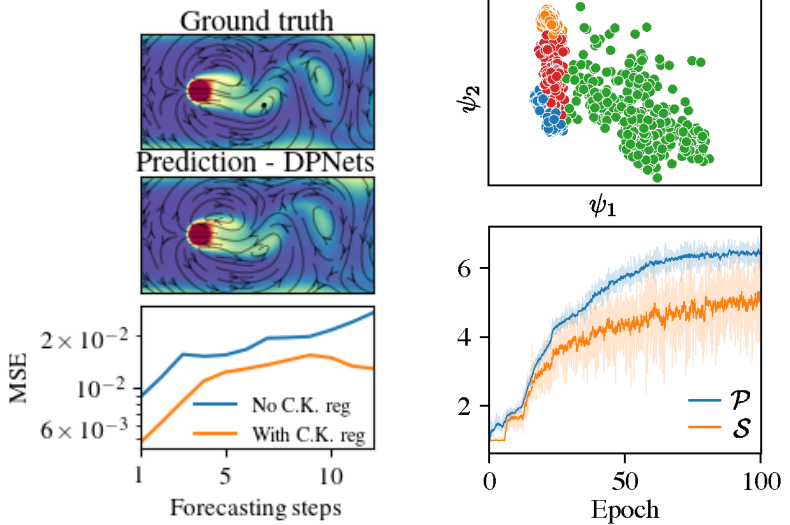


Figure 2: (Upper) Ground truth vs. DPNets forecast of the fluid state on test data. (Lower) Forecasting mean square error (MSE) as a function of the forecast horizon.

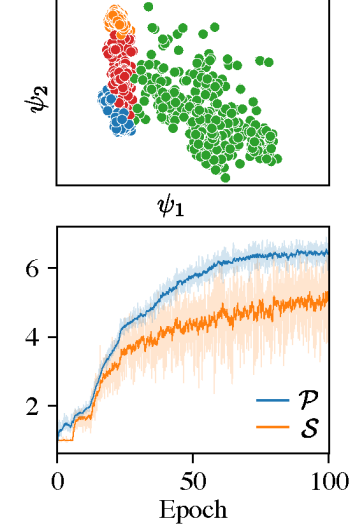


Figure 3: (Upper) Leading eigenfunctions evaluated on data reveal metastable states as clusters. (Lower) Training loop of DPNets. As expected, maximizing \mathcal{S} , drives \mathcal{P} up as well.

Continuous dynamics In this example, we showcase the effectiveness of DPNets on continuous dynamical systems, as discussed in Sec. 5, by investigating a one-dimensional SDE that describes the stochastic motion of a particle in a conservative force field. Here, the diffusion is just a constant $\sqrt{2\beta^{-1}}$, with β the “inverse temperature” of the system and the drift term is $-\nabla V(X_t)$, where $V : \mathbb{R} \rightarrow \mathbb{R}$ is the potential function $V(x) := 4(x^8 + 0.8e^{-80x^2} + 0.2e^{-80(x-0.5)^2} + 0.5e^{-40(x+0.5)^2})$ of [47]. The invariant distribution for this stochastic process is known as the Boltzmann distribution $\pi(dx) \propto e^{-\beta V(x)} dx$, see [47]. We sample X_t *non-uniformly*, where the time intervals between consecutive observations are drawn from a geometric distribution. Our objective is to accurately estimate the eigenvalues of the generator \mathcal{L} . The non-null eigenvalues of \mathcal{L} hold physical significance, as their (negative) inverse represents the average time for the particle to cross one of the system’s potential barriers [27]. We monitor the training of a DPNNet, and at any training step we use the current representation ψ_w to estimate eigenvalues of \mathcal{L}_w on validation dataset and them to the true eigenvalues of \mathcal{L} in Fig. 1. It is evident how, along the DPNNet training loop the embedding ψ_w is learned to accurately capture the invariant subspaces of the generator \mathcal{L} , thus yielding an improving eigenvalue estimation on the validation dataset.

The Metastable states of Chignolin: a real world example using GNNs The leading eigenfunctions of the transfer operator are themselves observables, describing the slowest modes of a dynamical system. In the context of molecular dynamics, such objects provide a simple characterization of the slowest (and usually most important) chemical processes occurring over the evolution of a chemical system. In this experiment we build from the work in [15] by employing our framework to learn the leading eigenfunctions associated to the dynamics of Chignolin, a folding protein, from a $106\ \mu\text{s}$ long molecular dynamics simulation sampled every 200 ps, totalling over half a million data points [33]. We consider every heavy atom for a total of 93 nodes as well as a cutoff radius of 6 Angstroms giving an average of 30 neighbours for each atom. Compared to [15], which selects only the $\approx 20 C_\alpha$ atoms each with its first 5 neighbours, our experiment has therefore a much larger scale. Indeed, [15] reports being able to train directly with the objective \mathcal{P} , while in our case we always encountered numerical errors, and we were able to only successfully train the \mathcal{S} objective. We parametrized

the feature map with a graph neural network (GNN) model. GNNs currently are the state of the art in modeling atomistic systems [11], and allow one to elegantly incorporate the roto-translational and permutational symmetries prescribed by physics. Specifically, we train a SchNet [44, 45] model with 3 interaction blocks, where in each block the latent atomic environment is 64-dimensional and the inter-atomic distances used for the message-passing step are expanded over 20 radial basis functions. After the last interaction block, each latent atomic environment is forwarded to a linear layer and then aggregated via averaging. The model has been trained for 100 epochs with an Adam optimizer and a learning rate of 10^{-3} . We have computed the eigenfunctions of the dynamics by fitting a standard Kernel Ridge estimator for the Koopman operator [26] over 4096 subsampled trajectory points and evaluating the resulting eigenfunctions (see Fig. 3). We analyzed the eigenfunctions using the technique described in [39], which links each metastable state to physically interpretable conformational descriptors. Our analysis aligns perfectly with [39], where the slowest metastable state corresponds to the folding-unfolding transition and is linked to the distance between residues (1, 10) and (2, 9) located at opposite ends of the protein. Additionally, the immediately faster metastable state represents a conformational change within the folded state, characterized by the relative angle between residues 6 and 8.

7 Conclusions

We propose a general framework for learning a latent representation of dynamical systems, based on orthogonal projections in data-spaces. This representation captures the principal invariant space of the transfer operator and can be applied to both discrete and continuous dynamical systems. The representations are learned through the optimization of a smooth objective function, which we have shown to be a tight relaxation of canonical correlation analysis. Extensive numerical experiments demonstrate the effectiveness and generality of DPNet in various settings, suggesting that they are a promising tool for data-driven dynamical systems. A limitation of this work is that the score functional for the continuous systems might be unstable since it leverages covariance matrix inversion. Moreover, in the future, it would be valuable to study the statistical learning properties of the algorithm presented here.

References

- [1] Alexander, R. and Giannakis, D. (2020). Operator-theoretic framework for forecasting nonlinear time series with kernel analog techniques. *Physica D: Nonlinear Phenomena*, 409:132520.
- [2] Allen, E. (2007). *Modeling with Itô stochastic differential equations*, volume 22. Springer Science & Business Media.
- [3] Andrew, G., Arora, R., Bilmes, J., and Livescu, K. (2013). Deep canonical correlation analysis. In *International Conference on Machine Learning*, pages 1247–1255. PMLR.
- [4] Arnold, L. (1974). *Stochastic Differential Equations: Theory and Applications*, volume 2. John Wiley & Sons.
- [5] Aronszajn, N. (1950). Theory of reproducing kernels. *Transactions of the American Mathematical Society*, 68(3):337–404.
- [6] Azencot, O., Erichson, N. B., Lin, V., and Mahoney, M. (2020). Forecasting sequential data using consistent koopman autoencoders. In *International Conference on Machine Learning*, pages 475–485. PMLR.
- [7] Bevanda, P., Beier, M., Kerz, S., Lederer, A., Sosnowski, S., and Hirche, S. (2021). KoopmanizingFlows: Diffeomorphically Learning Stable Koopman Operators. *arXiv preprint arXiv:2112.04085*.
- [8] Bouvrie, J. and Hamzi, B. (2017). Kernel Methods for the Approximation of Nonlinear Systems. *SIAM Journal on Control and Optimization*, 55(4):2460–2492.
- [9] Brunton, S. L., Budišić, M., Kaiser, E., and Kutz, J. N. (2022). Modern Koopman Theory for Dynamical Systems. *SIAM Review*, 64(2):229–340.
- [10] Cannarsa, P., Mansutti, D., and Provenzale, A. (2020). *Mathematical Approach to Climate Change and Its Impacts: MAC2I*, volume 38. Springer.
- [11] Chanussot, L., Das, A., Goyal, S., Lavril, T., Shuaibi, M., Riviere, M., Tran, K., Heras-Domingo, J., Ho, C., Hu, W., Palizhati, A., Sriram, A., Wood, B., Yoon, J., Parikh, D., Zitnick, C. L., and Ulissi, Z. (2021). Open catalyst 2020 (OC20) dataset and community challenges. *ACS Catalysis*, 11(10):6059–6072.
- [12] Das, S. and Giannakis, D. (2020). Koopman spectra in reproducing kernel Hilbert spaces. *Applied and Computational Harmonic Analysis*, 49(2):573–607.

[13] Fan, F., Yi, B., Rye, D., Shi, G., and Manchester, I. R. (2021). Learning Stable Koopman Embeddings. *arXiv preprint arXiv.2110.06509*.

[14] Fisher, M., Nocedal, J., Trémole, Y., and Wright, S. J. (2009). Data assimilation in weather forecasting: a case study in pde-constrained optimization. *Optimization and Engineering*, 10(3):409–426.

[15] Ghorbani, M., Prasad, S., Klauda, J. B., and Brooks, B. R. (2022). GraphVAMPNet, using graph neural networks and variational approach to markov processes for dynamical modeling of biomolecules. *The Journal of Chemical Physics*, 156(18):184103.

[16] Golub, G. H. and Pereyra, V. (1973). The differentiation of pseudo-inverses and nonlinear least squares problems whose variables separate. *SIAM Journal on Numerical Analysis*, 10(2):413–432.

[17] Golub, G. H. and Van Loan, C. F. (2013). *Matrix Computations*. JHU press.

[18] Goodfellow, I., Bengio, Y., and Courville, A. (2016). *Deep Learning*. MIT press.

[19] Gorini, V. and Kossakowski, A. (1976). Completely positive dynamical semigroups of N-level systems. *Journal of Mathematical Physics*, 17(5):821.

[20] Gretton, A., Bousquet, O., Smola, A., and Schölkopf, B. (2005). Measuring statistical dependence with hilbert-schmidt norms. In *Algorithmic Learning Theory: 16th International Conference, ALT 2005, Singapore, October 8-11, 2005. Proceedings 16*, pages 63–77. Springer.

[21] Hardoon, D. R., Szedmak, S., and Shawe-Taylor, J. (2004). Canonical correlation analysis: An overview with application to learning methods. *Neural Computation*, 16(12):2639–2664.

[22] Harold, H. (1936). Relations between two sets of variates. *Biometrika*, 28(3/4):321.

[23] Hoffmann, M., Scherer, M. K., Hempel, T., Mardt, A., de Silva, B., Husic, B. E., Klus, S., Wu, H., Kutz, J. N., Brunton, S., and Noé, F. (2021). Deeptime: a python library for machine learning dynamical models from time series data. *Machine Learning: Science and Technology*.

[24] Kawahara, Y. (2016). Dynamic Mode Decomposition with Reproducing Kernels for Koopman Spectral Analysis. In *Advances in Neural Information Processing Systems*, volume 29.

[25] Klus, S., Schuster, I., and Muandet, K. (2019). Eigendecompositions of transfer operators in reproducing kernel Hilbert spaces. *Journal of Nonlinear Science*, 30(1):283–315.

[26] Kostic, V., Novelli, P., Maurer, A., Ciliberto, C., Rosasco, L., and Pontil, M. (2022). Learning dynamical systems via Koopman operator regression in reproducing kernel hilbert spaces. In *Advances in Neural Information Processing Systems*.

[27] Kramers, H. (1940). Brownian motion in a field of force and the diffusion model of chemical reactions. *Physica*, 7(4):284–304.

[28] Kutz, J. N., Brunton, S. L., Brunton, B. W., and Proctor, J. L. (2016). *Dynamic Mode Decomposition*. Society for Industrial and Applied Mathematics.

[29] Lasota, A. and Mackey, M. C. (1994). *Chaos, Fractals, and Noise*, volume 97 of *Applied Mathematical Sciences*. Springer New York.

[30] Li, Q., Dietrich, F., Boltt, E. M., and Kevrekidis, I. G. (2017). Extended dynamic mode decomposition with dictionary learning: A data-driven adaptive spectral decomposition of the koopman operator. *Chaos: An Interdisciplinary Journal of Nonlinear Science*, 27(10):103111.

[31] Li, Z., Meunier, D., Mollenhauer, M., and Gretton, A. (2022). Optimal rates for regularized conditional mean embedding learning. In *Advances in Neural Information Processing Systems*.

[32] Lindblad, G. (1976). On the generators of quantum dynamical semigroups. *Communications in Mathematical Physics*, 48(2):119–130.

[33] Lindorff-Larsen, K., Piana, S., Dror, R. O., and Shaw, D. E. (2011). How fast-folding proteins fold. *Science*, 334(6055):517–520.

[34] Lusch, B., Kutz, J. N., and Brunton, S. L. (2018). Deep learning for universal linear embeddings of nonlinear dynamics. *Nature Communications*, 9(1).

[35] Mardt, A., Pasquali, L., No'e, F., and Wu, H. (2019). Deep learning markov and koopman models with physical constraints. In *Mathematical and Scientific Machine Learning*.

[36] Mardt, A., Pasquali, L., Wu, H., and Noé, F. (2018). Vampnets for deep learning of molecular kinetics. *Nature Communications*, 9(1):5.

[37] McCarty, J. and Parrinello, M. (2017). A variational conformational dynamics approach to the selection of collective variables in metadynamics. *The Journal of Chemical Physics*, 147(20):204109.

[38] Minsker, S. (2017). On some extensions of Bernstein's inequality for self-adjoint operators. *Statistics & Probability Letters*, 127:111–119.

[39] Novelli, P., Bonati, L., Pontil, M., and Parrinello, M. (2022). Characterizing metastable states with the help of machine learning. *Journal of Chemical Theory and Computation*, 18(9):5195–5202.

[40] Otto, S. E. and Rowley, C. W. (2019). Linearly recurrent autoencoder networks for learning dynamics. *SIAM Journal on Applied Dynamical Systems*, 18(1):558–593.

[41] Pascucci, A. (2011). *PDE and Martingale Methods in Option Pricing*. Springer Milan.

[42] Raissi, M., Yazdani, A., and Karniadakis, G. E. (2020). Hidden fluid mechanics: Learning velocity and pressure fields from flow visualizations. *Science*, 367(6481):1026–1030.

[43] Ross, S. M. (1995). *Stochastic Processes*. John Wiley & Sons.

[44] Schütt, K. T., Hessmann, S. S. P., Gebauer, N. W. A., Lederer, J., and Gastegger, M. (2023). SchNetPack 2.0: A neural network toolbox for atomistic machine learning. *The Journal of Chemical Physics*, 158(14):144801.

[45] Schütt, K. T., Kessel, P., Gastegger, M., Nicoli, K. A., Tkatchenko, A., and Müller, K.-R. (2019). SchNetPack: A Deep Learning Toolbox For Atomistic Systems. *Journal of Chemical Theory and Computation*, 15(1):448–455.

[46] Schütte, C., Huisenga, W., and Deuflhard, P. (2001). Transfer Operator Approach to Conformational Dynamics in Biomolecular Systems. In *Ergodic Theory, Analysis, and Efficient Simulation of Dynamical Systems*, pages 191–223. Springer Berlin Heidelberg.

[47] Schwantes, C. R. and Pande, V. S. (2015). Modeling Molecular Kinetics with tICA and the Kernel Trick. *Journal of Chemical Theory and Computation*, 11(2):600–608.

[48] Tian, W. and Wu, H. (2021). Kernel embedding based variational approach for low-dimensional approximation of dynamical systems. *Computational Methods in Applied Mathematics*, 21(3):635–659.

[49] Trefethen, L. N. and Embree, M. (2020). *Spectra and Pseudospectra: The Behavior of Nonnormal Matrices and Operators*. Princeton University Press.

[50] Tropp, J. A. (2012). User-friendly tail bounds for sums of random matrices. Technical report.

[51] Tuckerman, M. (2010). *Statistical Mechanics: Theory and Molecular Simulation*. Oxford university press.

[52] Wehmeyer, C. and Noé, F. (2018). Time-lagged autoencoders: Deep learning of slow collective variables for molecular kinetics. *The Journal of Chemical Physics*, 148(24):241703.

[53] Williams, M. O., Rowley, C. W., and Kevrekidis, I. G. (2015). A kernel-based method for data-driven Koopman spectral analysis. *Journal of Computational Dynamics*, 2(2):247–265.

[54] Wu, H. and Noé, F. (2019). Variational Approach for Learning Markov Processes from Time Series Data. *Journal of Nonlinear Science*, 30(1):23–66.

[55] Yeung, E., Kundu, S., and Hodas, N. (2019). Learning deep neural network representations for koopman operators of nonlinear dynamical systems. In *2019 American Control Conference (ACC)*. IEEE.

Appendix

The appendix is organized as follows.

- App. A reviews the notation used throughout the paper and basic notions of stochastic processes and reproducing kernel Hilbert spaces.
- In App. B we present the theoretical background for material presented in Sec. 2.
- In App. C we prove the first main result of the paper, Thm. 1.
- App. D adds value to Sec. 4. We first give theoretical justification for using the empirical score instead of the population one, and then provide details on how to address downstream tasks.
- In App. E we prove the second main result of the paper, Thm. 2 about DPNets for continuous time stochastic processes.
- Finally, App. F contains more information about the experiments as well as additional results.

A Background and notation

A.1 Stochastic processes tools

Let \mathcal{X} be a state space and $\Sigma_{\mathcal{X}}$ be the Borel σ -algebra on \mathcal{X} . Let \mathcal{M} denote the space of all finite measures on $(\mathcal{X}, \Sigma_{\mathcal{X}})$. In what follows, we consider a random process $(X_t)_{t \in \mathbb{T}}$ with values in a state space \mathcal{X} .

Definition 1 (Markov process.). *Let $\mathcal{F}_t := \Sigma(\{X_s : 0 \leq s \leq t\})$ be the sigma-algebra generated by the elements of the process up to time t . The random process $\mathbf{X} = (X_t)_{t \in \mathbb{T}}$ is called a Markov process if for all $t, \tau \geq 0$ and $B \in \Sigma_{\mathcal{X}}$ it holds*

$$\mathbb{P}(X_{t+\tau} \in B | \mathcal{F}_t) = \mathbb{P}(X_{t+\tau} \in B | X_t), \quad (24)$$

that is, conditioning on the full history of the process \mathcal{F}_t up to time t is equivalent to condition only on the state of the process at time t . For this reason, Markov process are sometimes called “memoryless”.

Definition 2. The transition density function $p_{\tau} : \mathcal{X} \times \mathcal{X} \rightarrow [0, \infty]$ of a time-homogeneous process \mathbf{X} is defined by

$$\mathbb{P}(X_{t+\tau} \in B | X_t = x) = \int_B p_{\tau}(x, y) dy,$$

for every measurable set $B \in \Sigma_{\mathcal{X}}$.

The distribution of a time-homogeneous stochastic process $(X_t)_t$ with transition density functions $(p_{\tau})_{\tau > 0}$ can be described by the semigroup of transfer operators $(\mathcal{T}_{\tau})_{\tau \geq 0}$ usually defined on $L^{\infty}(\mathcal{X})$.

Definition 3 (Transfer operator). For any $\tau \geq 0$, the Koopman transfer operator $\mathcal{T}_{\tau} : L^{\infty}(\mathcal{X}) \rightarrow L^{\infty}(\mathcal{X})$ is defined by

$$\mathcal{T}_{\tau}(f) = \mathbb{E}[f(X_{t+\tau}) | X_t = \cdot], \quad \forall f \in L^{\infty}(\mathcal{X}).$$

Definition 4 (Feller process). Let $(\mathcal{T}_{\tau})_{\tau \geq 0}$ be the semigroup of transfer operators of a homogeneous Markov process. Then, $(\mathcal{T}_{\tau})_{\tau \geq 0}$ is said to be a Feller semigroup when the following condition holds:

1. $\mathcal{T}_{\tau}(\mathcal{C}_0(\mathcal{X})) \subseteq \mathcal{C}_0(\mathcal{X})$ for all $\tau \geq 0$.
2. $\lim_{t \rightarrow 0} \|\mathcal{T}_{\tau} f - f\| = 0$ for all $f \in \mathcal{C}_0(\mathcal{X})$.

Here $\mathcal{C}_0(\mathcal{X})$ is the Banach space of all continuous functions vanishing at infinity.

Definition 5 (Infinitesimal generator of a semigroup). Let $(\mathcal{T}_{\tau})_{\tau \geq 0}$ be a Feller semigroup. We define its infinitesimal generator $\mathcal{L} : \mathcal{C}_0(\mathcal{X}) \rightarrow \mathcal{C}_0(\mathcal{X})$

$$\mathcal{L}f = \lim_{\tau \rightarrow 0} \frac{1}{\tau} (\mathcal{T}_{\tau} f - f),$$

for any $f \in \mathcal{C}_0(\mathcal{X})$ such that the above limit is well-defined.

The above definitions can be lifted to $L^2_{\mu}(\mathcal{X})$ if the dynamical system has an invariant distribution, or if we are interested in the action of \mathcal{T}_{τ} on a specific couple of states X, X' of the process, as discussed in the main text.

A.2 Reproducing kernel Hilbert spaces

In this section we review few basic concepts on kernel based approaches to learning transfer operators; for more details on reproducing kernel Hilbert spaces (RKHS) we refer reader to [5].

Let $k_X: \mathcal{X} \times \mathcal{X} \rightarrow \mathbb{R}$ and $k_{X'}: \mathcal{X} \times \mathcal{X} \rightarrow \mathbb{R}$ be two bounded kernels, and let \mathcal{H} and \mathcal{H}' be their respective reproducing kernel Hilbert spaces (RKHS). Denote the canonical feature maps by $\phi_X(x) := k_X(x, \cdot)$, $x \in \mathcal{X}$, and $\phi_{X'}(x') := k_{X'}(x', \cdot)$, $x' \in \mathcal{X}$.

Next, consider two probability measures μ and μ' on \mathcal{X} , and their associated L^2 spaces $L^2_\mu(\mathcal{X})$ and $L^2_{\mu'}(\mathcal{X})$. If $k_X(\cdot, \cdot)$ is square-integrable w.r.t. measure μ and $k_{X'}(\cdot, \cdot)$ is square-integrable w.r.t. the measure μ' , then we can define injection (or the evaluation) operators $S_\mu: \mathcal{H} \hookrightarrow L^2_\mu(\mathcal{X})$ and $S_{\mu'}: \mathcal{H}' \hookrightarrow L^2_{\mu'}(\mathcal{X})$. Then, their adjoints $S_\mu^*: L^2_\mu(\mathcal{X}) \rightarrow \mathcal{H}$ and $S_{\mu'}^*: L^2_{\mu'}(\mathcal{X}) \rightarrow \mathcal{H}'$ are given by

$$S_\mu^* f = \int_{\mathcal{X}} f(x) \phi_X(x) \mu(dx) \in \mathcal{H} \quad \text{and} \quad S_{\mu'}^* f' = \int_{\mathcal{X}} f'(x') \phi_{X'}(x') \mu'(dx') \in \mathcal{H}',$$

where $f \in L^2_\mu(\mathcal{X})$ and $f' \in L^2_{\mu'}(\mathcal{X})$.

Using injections and their adjoints one can introduce covariance operators $C_X: \mathcal{H} \rightarrow \mathcal{H}$ and $C_{X'}: \mathcal{H}' \rightarrow \mathcal{H}'$ by

$$C_X := S_\mu^* S_\mu = \mathbb{E}_{X \sim \mu} \phi_X(X) \otimes \phi_X(X), \quad \text{and} \quad C_{X'} := S_{\mu'}^* S_{\mu'} = \mathbb{E}_{X' \sim \mu'} \phi_{X'}(X') \otimes \phi_{X'}(X'),$$

as well as the cross-covariance $C_{XX'}: \mathcal{H}' \rightarrow \mathcal{H}$ operator

$$C_{XX'} := S_\mu^* \mathcal{T} S_{\mu'} = \mathbb{E}_{(X, X') \sim \rho} \phi_X(X) \otimes \phi_{X'}(X'),$$

where ρ is the joint measure of (X, X') and $\mathcal{T}: L^2_{\mu'}(\mathcal{X}) \rightarrow L^2_\mu(\mathcal{X})$ is a transfer operator corresponding to the evolution of $X \sim \mu$ to $X' \sim \mu'$.

Different estimators for the problem of learning transfer operators from data $\mathcal{D} = (x_i, x'_i)_{i \in [n]}$ have been considered, see e.g. [26, 31], which are all of the form $\widehat{T}_W = \widehat{S}'^* W \widehat{S}$, where $W \in \mathbb{R}^{n \times n}$ and $\widehat{S}: \mathcal{H} \rightarrow \mathbb{R}^n$ and $\widehat{S}': \mathcal{H}' \rightarrow \mathbb{R}^n$ are sampling operators given by $\widehat{S}f = n^{-\frac{1}{2}}[f(x_1) \dots f(x_n)]^\top$, $f \in \mathcal{H}$, and $\widehat{S}'f' = n^{-\frac{1}{2}}[f'(x'_1) \dots f'(x'_n)]^\top$, $f' \in \mathcal{H}'$. In particular, kernel methods usually consider *universal kernels* that generate infinite-dimensional RKHS spaces that are dense in L^2 . In such a way, one can approximate transfer operators via operator (vector-valued) regression arbitrarily well with enough data. In what follows, we are interested in finding finite-dimensional RKHS spaces based on DNN on which operator regression will lead to good estimation of the transfer operators.

B Problem and approach

In this section we first show how Eckart-Young's theorem justifies (4), which is the basis of Thm. 1.

Lemma 1. *Let \mathcal{H}_1 and \mathcal{H}_2 be two separable Hilbert spaces, and $A: \mathcal{H}_1 \rightarrow \mathcal{H}_2$ be a compact operator. Let $r \in \mathbb{N}$ and $\mathcal{P}_k^r := \{P: \mathcal{H}_k \rightarrow \mathcal{H}_k \mid P^* = P^2 = P, \text{rank}(P) \leq r\}$ denote the set of rank- r orthogonal projectors in \mathcal{H}_k , $k = 1, 2$.*

$$(i) \quad \max_{(P_1, P_2) \in \mathcal{P}_1^r \times \mathcal{P}_2^r} \|P_2 A P_1\|_{\text{HS}}^2 = \sum_{i \in [r]} \sigma_i^2(A),$$

$$(ii) \quad \text{Let } U_r \Sigma_r V_r^* \text{ be the } r\text{-truncated SVD of } A, \text{ then } (U_r U_r^*, V_r V_r^*) \in \arg \max_{(P_1, P_2) \in \mathcal{P}_1^r \times \mathcal{P}_2^r} \|P_2 A P_1\|_{\text{HS}}^2.$$

$$(iii) \quad \text{If } \sigma_{r+1}(A) < \sigma_r(A) \text{ and } \|A\|_{\text{HS}} < \infty, \text{ then } \arg \max_{(P_1, P_2) \in \mathcal{P}_1^r \times \mathcal{P}_2^r} \|P_2 A P_1\|_{\text{HS}}^2 \text{ is singleton.}$$

Proof. This lemma is a direct consequence of the Eckart-Young theorem for compact operators. Recall, since A is compact, there exists its SVD $A = U \Sigma V^*$ and Eckart-Young theorem states that if A is Hilbert-Schmidt, for every $r \in \mathbb{N}$ and every $B: \mathcal{H}_1 \rightarrow \mathcal{H}_2$ such that $\text{rank}(B) \leq r$, it holds $\|A - B\|_{\text{HS}} \geq \|A - A_r\|_{\text{HS}}$, where $A_r := U_r \Sigma_r V_r^*$ denotes the r -truncated SVD of A . Moreover, if $\sigma_{r+1}(A) < \sigma_r(A)$, then equality implies $B = A_r$.

Hence, for arbitrary $P_k \in \mathcal{P}_k^r$, $k = 1, 2$, using that the norm of a projection is 1 and Pythagoras theorem, for every $m \geq r$ we have that

$$\begin{aligned} \|P_2 A_m P_1\|_{\text{HS}}^2 &\leq \|P_2 A_m\|_{\text{HS}}^2 \|P_1\|^2 = \|P_2 A_m\|_{\text{HS}}^2 = \|A_m\|_{\text{HS}}^2 - \|[I - P_2] A_m\|_{\text{HS}}^2 \\ &= \|A_m\|_{\text{HS}}^2 - \|A_m - P_2 A_m\|_{\text{HS}}^2 \leq \|A_m\|_{\text{HS}}^2 - \|A_m - A_r\|_{\text{HS}}^2 = \|A_r\|_{\text{HS}}^2, \end{aligned}$$

and, similarly, $\|P_2 A_m P_1\|_{\text{HS}}^2 \leq \|A_m\|_{\text{HS}}^2 - \|A_m - A_m P_1\|_{\text{HS}}^2 \leq \|A_r\|_{\text{HS}}^2$. However, since

$$\begin{aligned} \|\|P_2 A P_1\|_{\text{HS}} - \|P_2 A_m P_1\|_{\text{HS}}\| &\leq \|P_2(A - A_m)P_1\|_{\text{HS}} \leq \sqrt{r}\|P_2(A - A_m)P_1\| \\ &\leq \sqrt{r}\|A - A_m\| \leq \sqrt{r}\sigma_{m+1}(A), \end{aligned}$$

we obtain $\|P_2 A P_1\|_{\text{HS}}^2 \leq \|A_r\|_{\text{HS}}^2 + \sqrt{r}\sigma_{m+1}(A)$ for all $m \geq r$. Thus, since $\|P_2 A P_1\|_{\text{HS}}^2 = \|A_r\|_{\text{HS}}^2$ obviously holds for $P_1 = V_r V_r^*$ and $P_2 = U_r U_r^*$, letting $m \rightarrow \infty$ we obtain ((i)) and ((ii)).

Finally, assume that A is an Hilbert-Schmidt operator such that $0 \leq \sigma_{r+1}(A) < \sigma_r(A)$. Then, similarly to the above now working with A instead of A_m ,

$$\|P_2 A P_1\|_{\text{HS}}^2 \leq \|A\|_{\text{HS}}^2 - \max\{\|A - A P_1\|_{\text{HS}}^2, \|A - P_2 A\|_{\text{HS}}^2\} \leq \|A_r\|_{\text{HS}}^2.$$

So, if

$$(P_1, P_2) \in \arg \max_{(P'_1, P'_2) \in \mathcal{P}'_1 \times \mathcal{P}'_2} \|P'_2 A P'_1\|_{\text{HS}}^2,$$

then

$$\max\{\|A - A P_1\|_{\text{HS}}^2, \|A - P_2 A\|_{\text{HS}}^2\} = \|A - A_r\|_{\text{HS}}^2.$$

Now, the uniqueness result of the Eckart-Young theorem implies that $A P_1 = P_2 A = A_r$, and, consequently $\text{rank}(P_1) = \text{rank}(P_2) = r$, $A_r^\dagger A P_1 = A_r^\dagger A_r$ and $P_2 A A_r^\dagger = A_r A_r^\dagger$. Therefore, $V_r V_r^* P_1 = V_r V_r^*$ and $P_2 U_r U_r^* = U_r U_r^*$, imply $\text{Im}(P_1) \subseteq \text{Im}(V_r)$ and $\text{Im}(P_2) \subseteq \text{Im}(U_r)$. But since P_1 and P_2 have exactly rank r , we obtain $P_1 = V_r V_r^*$ and $P_2 = U_r U_r^*$. \square

Next, in the following Lemma we prove (7), relating the projection score with the covariance operators.

Lemma 2. *Let X and X' be two \mathcal{X} -valued random variables distributed according to probability measures μ and μ' , respectively. Given $w \in \mathcal{W}$ let for every $j \in [r]$ functions $\psi_{w,j}: \mathcal{X} \rightarrow \mathbb{R}$ and $\psi'_{w,j}: \mathcal{X} \rightarrow \mathbb{R}$ be square integrable w.r.t measures μ and μ' , respectively. If $P_{\mathcal{H}_w}: L^2_\mu(\mathcal{X}) \rightarrow L^2_\mu(\mathcal{X})$ and $P'_{\mathcal{H}'_w}: L^2_{\mu'}(\mathcal{X}) \rightarrow L^2_{\mu'}(\mathcal{X})$ are orthogonal projections onto subspaces $\mathcal{H}_w := \text{span}(\psi_{w,j})_{j \in [r]}$ and $\mathcal{H}'_w := \text{span}(\psi'_{w,j})_{j \in [r]}$, respectively, then*

$$\|P_{\mathcal{H}_w} \mathcal{T} P'_{\mathcal{H}'_w}\|_{\text{HS}}^2 = \|(C_X^w)^{\dagger/2} C_{XX'}^w (C_{X'}^w)^{\dagger/2}\|_{\text{HS}}^2. \quad (25)$$

Proof. The proof directly follows from the notion of finite-dimensional RKHS. Let $k_X^w: \mathcal{X} \times \mathcal{X} \rightarrow \mathbb{R}$ and $k_{X'}^w: \mathcal{X} \times \mathcal{X} \rightarrow \mathbb{R}$ be two kernels given by

$$k_X^w(x, y) := \psi_w(x)^\top \psi_w(y) \quad \text{and} \quad k_{X'}^w(x, y) := \psi'_{w,j}(x)^\top \psi'_{w,j}(y), \quad x, y \in \mathcal{X}.$$

Then \mathcal{H}_w and \mathcal{H}'_w are the reproducing kernel Hilbert spaces (RKHS) associated with kernels k_X^w and $k_{X'}^w$, respectively.

Now, due to square integrability of the embeddings $\psi_{w,j}$ and $\psi'_{w,j}$, $j \in [r]$, we have that the injection operators of the two RKHS spaces into their respective L^2 spaces are well-defined: $S_\mu: \mathcal{H}_w \hookrightarrow L^2_\mu(\mathcal{X})$ and $S_{\mu'}: \mathcal{H}'_w \hookrightarrow L^2_{\mu'}(\mathcal{X})$. Moreover, observing that \mathcal{H}_w and \mathcal{H}'_w are isometrically isomorphic to \mathbb{R}^r , we have that $S_\mu^* S_\mu: \mathcal{H}_w \rightarrow \mathcal{H}_w$ and $S_{\mu'}^* S_{\mu'}: \mathcal{H}'_w \rightarrow \mathcal{H}'_w$ can be identified with $C_X^w \in \mathbb{R}^{r \times r}$ and $C_{X'}^w \in \mathbb{R}^{r \times r}$, respectively, i.e.

$$S_\mu^* S_\mu = Q C_X^w Q^* \quad \text{and} \quad S_{\mu'}^* S_{\mu'} = Q' C_{X'}^w (Q')^*.$$

where $Q: \mathbb{R}^r \rightarrow \mathcal{H}_w$ and $Q': \mathbb{R}^r \rightarrow \mathcal{H}'_w$ are partial isometries, meaning that $Q Q^*$ and $Q' (Q')^*$ are identity operators on \mathcal{H}_w and $Q^* Q$ and $(Q')^* Q'$ are identity matrices in $\mathbb{R}^{r \times r}$.

As a consequence, the polar decompositions of finite rank operators S_μ and $S_{\mu'}$ can be written as

$$S_\mu = U Q (C_X^w)^{1/2} Q^* \quad \text{and} \quad S_{\mu'} = U' Q' (C_{X'}^w)^{1/2} (Q')^*, \quad (26)$$

where $U: \mathcal{H}_w \rightarrow L^2_\mu(\mathcal{X})$ and $U': \mathcal{H}'_w \rightarrow L^2_{\mu'}(\mathcal{X})$ are partial isometries.

But then, since \mathcal{H}_w as a subspace of $L^2_\mu(\mathcal{X})$ is identified as $\text{Im}(S_\mu)$, and \mathcal{H}'_w as a subspace of $L^2_{\mu'}(\mathcal{X})$ is identified as $\text{Im}(S_{\mu'})$, using adjoints $S_\mu^*: L^2_\mu(\mathcal{X}) \rightarrow \mathcal{H}_w$ and $S_{\mu'}^*: L^2_{\mu'}(\mathcal{X}) \rightarrow \mathcal{H}'_w$, we can write the aforementioned orthogonal projections as

$$P_{\mathcal{H}_w} = S_\mu (S_\mu^* S_\mu)^\dagger S_\mu^* \quad \text{and} \quad P_{\mathcal{H}'_w} = S_{\mu'} (S_{\mu'}^* S_{\mu'})^\dagger S_{\mu'}^*, \quad (27)$$

which, using (26) and the fact that $(C_X^w)^{1/2} (C_X^w)^\dagger = (C_X^w)^\dagger/2$, is equivalent to

$$P_{\mathcal{H}_w} = U Q (C_X^w)^{\dagger/2} Q^* S_\mu^* \quad \text{and} \quad P_{\mathcal{H}'_w} = U' Q' (C_{X'}^w)^{\dagger/2} (Q')^* S_{\mu'}^*.$$

Finally, since for every $v \in \mathbb{R}^r$ we obtain

$$\begin{aligned} (Q^* S_\mu^* \mathcal{T} S_{\mu'} Q') v &= Q^* S_\mu^* (\mathcal{T} S_{\mu'} Q' v) = Q^* \int_{\mathcal{X}} \mu(dx) \phi_X^w(x) (\mathcal{T} S_{\mu'} Q' v)(x) \\ &= Q^* \int_{\mathcal{X}} \int_{\mathcal{X}} \mu(dx) p(x, dx') \phi_X^w(x) (Q' v)(x') \\ &= Q^* \int_{\mathcal{X} \times \mathcal{X}} \rho(dx, dx') \phi_X^w(x) (Q' v)(x') \end{aligned}$$

where ρ is joint measure of (X, X') and ϕ_X^w is the canonical feature map of k_X^w , i.e. $\phi_X^w(x) = k_X^w(\cdot, x)$, $x \in \mathcal{X}$. Next, using the reproducing property

$$\begin{aligned} (Q^* S_\mu^* \mathcal{T} S_{\mu'} Q') v &= Q^* \int_{\mathcal{X} \times \mathcal{X}} \rho(dx, dx') \phi_X^w(x) \langle \phi_{X'}^w(x'), Q' v \rangle_{\mathcal{H}'_w} \\ &= \left[\int_{\mathcal{X} \times \mathcal{X}} \rho(dx, dx') Q^* \phi_X^w(x) \otimes ((Q')^* \phi_{X'}^w(x')) \right] v \\ &= \left[\int_{\mathcal{X} \times \mathcal{X}} \rho(dx, dx') \psi_w(x) \otimes \psi_w'(x') \right] v = C_{XX'}^w v, \end{aligned}$$

where $\phi_{X'}^w$ is the canonical feature map of $k_{X'}^w$, and we used that $Q^* \phi_X^w(x) = \psi_w(x)$ and $(Q')^* \phi_{X'}^w(x') = \psi_w'(x')$.

Therefore, using (27) we obtain

$$P_{\mathcal{H}_w} \mathcal{T} P'_{\mathcal{H}'_w} = U Q (C_X^w)^{\dagger/2} C_{XX'}^w (C_{X'}^w)^{\dagger/2} (Q')^* (U')^*,$$

which using that U, U' and Q, Q' are partial isometries, implies (25). \square

Finally, we discuss how to extend part of the analysis to the important setting of stationary deterministic systems for which the transfer operator is not compact.

Remark 1. *The compactness assumption on the transfer operator, does not hold for purely deterministic dynamical systems. However, our approach is still applicable to the study of deterministic systems on the attractor, i.e. when $X_{t+1} = F(X_t)$, for a deterministic map $F: \mathcal{X} \rightarrow \mathcal{X}$, and $X_t \sim \pi$ for all $t \in \mathbb{T}$, where π is the invariant measure defined on the attractor. Then, we have that $\mathbb{E}[f(X_{t+1}) | X_t] = F \circ f$ and $\mathcal{T}: L_\pi^2(\mathcal{X}) \rightarrow L_\pi^2(\mathcal{X})$ is unitary, see e.g. [9]. Thus, \mathcal{T} is not a compact operator, however it is a normal one. But then, recalling (2) and using the Pythagoras theorem, we get*

$$\inf_{w \in \mathcal{W}} \|[I - P_{\mathcal{H}_w}] \mathcal{T} P_{\mathcal{H}_w}\|_{\text{HS}}^2 = \inf_{w \in \mathcal{W}} \left(\|\mathcal{T} P_{\mathcal{H}_w}\|_{\text{HS}}^2 - \|P_{\mathcal{H}_w} \mathcal{T} P_{\mathcal{H}_w}\|_{\text{HS}}^2 \right) = r - \sup_{w \in \mathcal{W}} \mathcal{P}(w),$$

where the second equality holds since the HS-norm is unitarily invariant. Therefore, when w is such that $\mathcal{T} \psi_{w,j} = \lambda_j \psi_{w,j}$, since \mathcal{T} is unitary we have $\mathcal{P}(w) = \sum_{j=1}^r |\lambda_j| = r$ and the above inf is zero. Consequently, we have identified an r -dimensional invariant subspace of \mathcal{T} .

C Score functional

In this section, using Lem. 1, we prove one of the main theoretical results of the paper.

Theorem 1. *Let $\mathcal{T}: L_\mu^2(\mathcal{X}) \rightarrow L_\mu^2(\mathcal{X})$ be compact. If $\mathcal{H}_w \subseteq L_\mu^2(\mathcal{X})$ and $\mathcal{H}'_w \subseteq L_{\mu'}^2(\mathcal{X})$, then for all $\gamma \geq 0$*

$$\mathcal{S}^\gamma(w) \leq \mathcal{P}^\gamma(w) \leq \sigma_1^2(\mathcal{T}) + \dots + \sigma_r^2(\mathcal{T}). \quad (11)$$

Moreover, if $(\psi_{w,j})_{j \in [r]}$ and $(\psi'_{w,j})_{j \in [r]}$ are leading r left and right singular functions of \mathcal{T} , respectively, then both equalities in (11) hold. Finally, if the operator \mathcal{T} is Hilbert-Schmidt, $\sigma_r(\mathcal{T}) > \sigma_{r+1}(\mathcal{T})$ and $\gamma > 0$, then the “only if” relation is satisfied up to unitary equivalence.

Proof. Recall that $\mathcal{S}(w) := \|C_{XX'}^w\|_{\text{HS}}^2 / (\|C_X^w\| \|C_{X'}^w\|)$ and $\mathcal{P}^\gamma(w) = \mathcal{P}(w) - \gamma (\mathcal{R}(C_X^w) + \mathcal{R}(C_{X'}^w))$ with $\mathcal{P}(w) = \|P_{\mathcal{H}_w} \mathcal{T} P'_{\mathcal{H}'_w}\|_{\text{HS}}^2 = \|(C_X^w)^{\dagger/2} C_{XX'}^w (C_{X'}^w)^{\dagger/2}\|_{\text{HS}}^2$, where the last equality follows from Lemma 2. The first inequality in (2) holds thanks to a standard matrix norm inequality, while the second holds by applying Lemma 1(i) and noting that $\mathcal{R}(C_X^w) + \mathcal{R}(C_{X'}^w) \geq 0$.

Now assume that $(\psi_{w,j})_{j \in [r]}$ and $(\psi'_{w,j})_{j \in [r]}$ are some leading r left and right singular functions of \mathcal{T} , respectively. Then, since singular functions form ortho-normal systems in L^2 spaces we have that

$$(C_X^w)_{i,j} = \langle \psi_{w,i}, \psi_{w,j} \rangle_{L^2_\mu(\mathcal{X})} = \delta_{i,j} \quad \text{and} \quad (C_{X'}^w)_{i,j} = \langle \psi'_{w,i}, \psi'_{w,j} \rangle_{L^2_\mu(\mathcal{X})} = \delta_{i,j}, \quad i, j \in [r],$$

i.e. $C_X^w = C_{X'}^w = I_r$, and, therefore, $\mathcal{R}(C_X^w) = \mathcal{R}(C_{X'}^w) = 0$ and $\mathcal{S}(w) = \mathcal{P}(w)$. Thus, using Lemma 1(ii), we obtain that (11) holds with equalities in place of inequalities.

Next, assume that the operator \mathcal{T} is Hilbert-Schmidt, $\sigma_r(\mathcal{T}) > \sigma_{r+1}(\mathcal{T})$, $\gamma > 0$ and $\mathcal{S}^\gamma(w) = \sigma_1^2(\mathcal{T}) + \dots + \sigma_r^2(\mathcal{T})$. Then, clearly $\mathcal{R}(C_X^w) = \mathcal{R}(C_{X'}^w) = 0$, which implies that $C_X^w = C_{X'}^w = I_r$, i.e. $(\psi_{w,j})_{j \in [r]}$ and $(\psi'_{w,j})_{j \in [r]}$ form orthonormal systems. Consequently,

$$P_{\mathcal{H}_w} = \sum_{i \in [r]} \psi_{w,i} \otimes \psi_{w,i} \quad \text{and} \quad P_{\mathcal{H}'_w} = \sum_{i \in [r]} \psi'_{w,i} \otimes \psi'_{w,i},$$

and

$$\mathcal{P}(w) = \mathcal{P}^\gamma(w) = \mathcal{S}^\gamma(w) = \sigma_1^2(\mathcal{T}) + \dots + \sigma_r^2(\mathcal{T}).$$

But then, Lemma 1(iii) implies that $P_{\mathcal{H}_w}$ and $P_{\mathcal{H}'_w}$ are orthogonal projectors on the leading r left and right singular spaces of \mathcal{T} . In other words, up to unitary changes of basis, $(\psi_{w,j})_{j \in [r]}$ and $(\psi'_{w,j})_{j \in [r]}$ are leading r left and right singular functions of \mathcal{T} , which completes the proof. \square

We conclude this section with a remark on the importance of regularization.

Remark 2. *Recalling the proof of the previous theorem, note that when $\gamma = 0$, equality in (11) is achieved whenever \mathcal{H}_w and \mathcal{H}'_w are spanned by leading r left and right singular functions of \mathcal{T} , respectively. Meaning that after the change of basis $Q, Q' \in \mathbb{R}^{r \times r}$ so that $(\sum_{i \in [r]} Q_{i,j} \psi_{w,i})_{j \in [r]}$ and $(\sum_{i \in [r]} Q'_{i,j} \psi'_{w,i})_{j \in [r]}$ are leading left and right singular functions, respectively. Under the additional conditions, also the "only if" part holds for some changes of basis. Indeed, we can take the change of basis to be $Q = (C_X^w)^{-1/2}$ and $Q' = (C_{X'}^w)^{-1/2}$, which without regularization term, need not be unitary. This, as we see in Appendix D.2, highly impacts on the stability of computation of the transfer operator estimators, and, therefore, impacts their practical use.*

D Methods

D.1 Statistical learning guarantees

In this section, our goal is to derive concentration guarantees for the empirical score $\hat{\mathcal{S}}$ from the true score \mathcal{S} . We focus on time-homogeneous Markovian dynamical systems in the stationary regime with invariant measure π which was proposed in [26, 29].

Recall the definition of the true and empirical scores

$$\mathcal{S}(w) := \frac{\|C_{XX'}^w\|_{\text{HS}}^2}{\|C_X^w\| \|C_{X'}^w\|} \quad \text{and} \quad \hat{\mathcal{S}}(w) := \frac{\|\hat{C}_{XX'}^w\|_{\text{HS}}^2}{\|\hat{C}_X^w\| \|\hat{C}_{X'}^w\|}, \quad (28)$$

where \hat{C}_X^w , $\hat{C}_{X'}^w$, and $C_{XX'}^w$, are defined in (14)-(15). Denote by ρ the joint distribution of (X, X') .

We assume that the embeddings are bounded almost surely, that is there exists an absolute constant c such that

$$\sup_x \|\psi_w(x)\|^2 \leq c, \quad \sup_x \|\psi'_w(y)\|^2 \leq c. \quad (29)$$

For any fixed w and any fixed $\delta \in (0, 1)$, we assume that n is large enough such that

$$\frac{4c}{3 \|C_X^w\| n} \log(12r\delta^{-1}) + \sqrt{\frac{2}{\|C_X^w\| n} \log(12r\delta^{-1})} \leq \frac{1}{3}. \quad (30)$$

Define

$$\varepsilon_n(\delta) = \frac{4c}{3 \|C_X^w\| n} \log(12r\delta^{-1}) + \sqrt{\frac{2}{\|C_X^w\| n} \log(12r\delta^{-1})},$$

and

$$\varepsilon_n''(\delta) := c^2 \sqrt{\frac{5 \log(18\delta^{-1})}{n}} + c^2 \frac{C}{n},$$

where C is some absolute constant.

Theorem 3. *Let Conditions (29) and (30) be satisfied. Then we get with probability at least $1 - \delta$*

$$|\mathcal{S}(w) - \widehat{\mathcal{S}}(w)| \leq \mathcal{S}(w) \frac{3\varepsilon_n(\delta)}{1 - 3\varepsilon_n(\delta)} + \frac{\varepsilon_n''(\delta)}{\|C_X^w\| \|C_{X'}^w\| (1 - 3\varepsilon_n(\delta))}. \quad (31)$$

Proof. By definition of $\mathcal{S}(w)$ and $\widehat{\mathcal{S}}(w)$, we have

$$\begin{aligned} |\widehat{\mathcal{S}}(w) - \mathcal{S}(w)| &\leq \widehat{\mathcal{S}}(w) \left| \frac{\|\widehat{C}_X^w\| \|\widehat{C}_{X'}^w\| - \|C_X^w\| \|C_{X'}^w\|}{\|C_X^w\| \|C_{X'}^w\|} \right| + \left| \frac{\|\widehat{C}_{XX'}^w\|_{\text{HS}}^2 - \|C_{XX'}^w\|_{\text{HS}}^2}{\|C_X^w\| \|C_{X'}^w\|} \right| \\ &\leq |\widehat{\mathcal{S}}(w) - \mathcal{S}(w)| \left| \frac{\|\widehat{C}_X^w\| \|\widehat{C}_{X'}^w\| - \|C_X^w\| \|C_{X'}^w\|}{\|C_X^w\| \|C_{X'}^w\|} \right| + \mathcal{S}(w) \left| \frac{\|\widehat{C}_X^w\| \|\widehat{C}_{X'}^w\| - \|C_X^w\| \|C_{X'}^w\|}{\|C_X^w\| \|C_{X'}^w\|} \right| \\ &\quad + \left| \frac{\|\widehat{C}_{XX'}^w\|_{\text{HS}}^2 - \|C_{XX'}^w\|_{\text{HS}}^2}{\|C_X^w\| \|C_{X'}^w\|} \right|. \end{aligned}$$

Using (36), (38) below, we get with probability at least $1 - 2\delta$,

$$\left| \frac{\|\widehat{C}_X^w\| \|\widehat{C}_{X'}^w\| - \|C_X^w\| \|C_{X'}^w\|}{\|C_X^w\| \|C_{X'}^w\|} \right| \leq \varepsilon_n(\delta) + \varepsilon'_n(\delta) + \varepsilon_n(\delta) \varepsilon'_n(\delta).$$

Next, (39) gives with probability at least $1 - \delta$

$$\left| \frac{\|\widehat{C}_{XX'}^w\|_{\text{HS}}^2 - \|C_{XX'}^w\|_{\text{HS}}^2}{\|C_X^w\| \|C_{X'}^w\|} \right| \leq \frac{\varepsilon_n''(\delta)}{\|C_X^w\| \|C_{X'}^w\|}.$$

Under Conditions 29 and 30, we get

$$\varepsilon_n(\delta) = \varepsilon'_n(\delta) = \frac{4c}{3\|C_X^w\| n} \log(4r\delta^{-1}) + \sqrt{\frac{2}{\|C_X^w\| n} \log(4r\delta^{-1})} < \frac{1}{3},$$

and

$$\varepsilon_n''(\delta) := c^2 \sqrt{\frac{5 \log(6\delta^{-1})}{n}} + c^2 \frac{C}{n}.$$

An union bound gives with probability at least $1 - 3\delta$,

$$|\widehat{\mathcal{S}}(w) - \mathcal{S}(w)| \leq \mathcal{S}(w) \frac{3\varepsilon_n(\delta)}{1 - 3\varepsilon_n(\delta)} + \frac{\varepsilon_n''(\delta)}{\|C_X^w\| \|C_{X'}^w\| (1 - 3\varepsilon_n(\delta))}. \quad (32)$$

Replacing δ with $\delta/3$, we get the result with probability $1 - \delta$. \square

To control the operator norm deviation of the empirical covariances \widehat{C}_X^w and $\widehat{C}_{X'}^w$ from their population counterparts, we use the following dimension-free version of [38] of the non-commutative Bernstein inequality (see also Theorem 7.3.1 in [50] for an easier to read and slightly improved version) as well as an extension to self-adjoint Hilbert-Schmidt operators on separable Hilbert spaces.

Proposition 1 ([38] and Theorem 7.3.1 in [50]). *Let A_i , $i \in [n]$ be i.i.d copies of a random Hilbert-Schmidt operator A on separable Hilbert spaces. Let $\|A\| \leq c$ almost surely, $\mathbb{E}A = 0$ and let $\mathbb{E}[A^2] \preceq V$ for some trace class operator V . Then with probability at least $1 - \delta$*

$$\left\| \frac{1}{n} \sum_{i \in [n]} A_i \right\| \leq \frac{2c}{3n} \mathcal{L}_A(\delta) + \sqrt{\frac{2\|V\|}{n} \mathcal{L}_A(\delta)}, \quad (33)$$

where

$$\mathcal{L}_A(\delta) := \log \frac{4}{\delta} + \log \frac{\text{tr}(V)}{\|V\|}.$$

Proposition 2. Assume that $c_\psi := \sup_x \left\{ \|\psi_w(x)\|^2 \right\} < \infty$. Given $\delta > 0$, with probability in the i.i.d. draw of $(x_i)_{i=1}^n$ from μ , it holds that

$$\mathbb{P}\{\|\widehat{C}_X^w - C_X^w\|/\|C_X^w\| \leq \varepsilon_n(\delta)\} \geq 1 - \delta, \quad (34)$$

where

$$\varepsilon_n(\delta) := \frac{4c_\psi}{3\|C_X^w\|n} \mathcal{L}(\delta) + \sqrt{\frac{2}{\|C_X^w\|n} \mathcal{L}(\delta)} \quad \text{and} \quad \mathcal{L}(\delta) := \log \frac{4r}{\delta}. \quad (35)$$

Proof of Proposition 2. Proof follows directly from Proposition 1 applied to operators $\psi_w(x_i) \otimes \psi_w(x_i)$ using the fact that $C_X^w = \mathbb{E} \psi_w(x_i) \otimes \psi_w(x_i)$, where we recall that $\psi_w(x) := (\psi_{w,1}(x), \dots, \psi_{w,r}(x)) \in \mathbb{R}^r$. Hence, we have the obvious upper bound $\frac{\text{tr}(C_X^w)}{\|C_X^w\|} \leq r$. \square

We deduce from (34), with probability at least $1 - \delta$

$$(1 - \varepsilon_n(\delta))\|C_X^w\| \leq \|\widehat{C}_X^w\| \leq \|C_X^w\|(1 + \varepsilon_n(\delta))\|C_X^w\|, \quad (36)$$

A similar result is also valid for $\widehat{C}_{X'}^w$ provided that $c_{\psi'} := \sup_{w,x} \left\{ \|\psi'_w(x)\|^2 \right\} < \infty$. Define

$$\varepsilon'_n(\delta) := \frac{4c_{\psi'}}{3\|C_X^w\|n} \mathcal{L}(\delta) + \sqrt{\frac{2}{\|C_X^w\|n} \mathcal{L}(\delta)} \quad \text{and} \quad \mathcal{L}(\delta) := \log \frac{4r}{\delta}. \quad (37)$$

Then, with probability at least $1 - \delta$

$$(1 - \varepsilon'_n(\delta))\|C_{X'}^w\| \leq \|\widehat{C}_{X'}^w\| \leq (1 + \varepsilon'_n(\delta))\|C_{X'}^w\|, \quad (38)$$

We study now the deviation of $\|\widehat{C}_{XX'}^w\|_{\text{HS}}^2$ from $\|C_{XX'}^w\|_{\text{HS}}^2$. We can essentially apply Theorem 3 in [20] with kernels $k_w(x, x') = \langle \psi_w(x), \psi_w(x') \rangle$ and $l_w(y, y') = \langle \psi'_w(y), \psi'_w(y') \rangle$. Note that these two kernels are bounded. Indeed we have

$$\sup_{x,x'} |k_w(x, x')| \leq \sup_x \|\psi_w(x)\|^2 \leq c_\psi \quad \text{and} \quad \sup_{y,y'} |l_w(y, y')| \leq \sup_x \|\psi'_w(y)\|^2 \leq c_{\psi'}.$$

Hence, for any $n \geq 2$ and $\delta > 0$, we get with probability at least $1 - \delta$,

$$\left| \|\widehat{C}_{XX'}^w\|_{\text{HS}}^2 - \|C_{XX'}^w\|_{\text{HS}}^2 \right| \leq \epsilon''_n(\delta), \quad (39)$$

where

$$\epsilon''_n(\delta) := c_\psi c_{\psi'} \sqrt{\frac{5 \log(6\delta^{-1})}{n}} + c_\psi c_{\psi'} \frac{C}{n},$$

for some absolute constant $C > 0$.

D.2 Operator regression and prediction

We next discuss how to design an estimator of the transfer operator $\mathcal{T}: L_{\mu'}^2(\mathcal{X}) \rightarrow L_\mu^2(\mathcal{X})$ using the learned subspaces \mathcal{H}_w and \mathcal{H}'_w . Namely, we estimate $\mathcal{T} \approx \widehat{\mathcal{T}}_w: \mathcal{H}'_w \rightarrow \mathcal{H}_w$. The purpose of such estimation is to, given a initial state $x \in \mathcal{X}$, predict the average evolution $\mathbb{E}[f(X') | X = x]$ of an observable $f \in L_{\mu'}^2(\mathcal{X})$.

In what follows, let us assume that after the training we obtained $w \in \mathcal{W}$ such that C_X^w and $C_{X'}^w$ are invertible, i.e. that $(\psi_{w,j})_{j \in [r]} (\psi'_{w,j})_{j \in [r]}$ form basis of the spaces \mathcal{H}_w and \mathcal{H}'_w , respectively. This means that the operators $E_w: \mathbb{R}^r \mapsto \mathcal{H}_w$ and $E'_w: \mathbb{R}^r \mapsto \mathcal{H}'_w$ can be properly defined as partial isometries by $E_w v = \psi_w(\cdot)^\top v$ and $E'_w v = \psi'_w(\cdot)^\top v$. So, every estimator can be written in the form $\widehat{\mathcal{T}}_w = E_w \widehat{T}(E'_w)^*$ for some $\widehat{T} \in \mathbb{R}^{r \times r}$.

Different estimators can then be computed from data $\mathcal{D}_n := (x_i, x'_i)_{i \in [n]}$ (either seen or unseen during training time). To elaborate on this, let us, as usual for kernel methods, define the sampling operators $\widehat{S}: \mathcal{H}_w \rightarrow \mathbb{R}^n$ and $\widehat{S}': \mathcal{H}'_w \rightarrow \mathbb{R}^n$, given by $\widehat{S}h = n^{-\frac{1}{2}}[h(x_1) \dots h(x_n)]^\top$, $h \in \mathcal{H}_w$, and $\widehat{S}'g = n^{-\frac{1}{2}}[g(x'_1) \dots g(x'_n)]^\top$, $g \in \mathcal{H}'_w$. Notice that we can extend the domain of definition of these operators via interpolation to arbitrary functions $\mathcal{X} \rightarrow \mathbb{R}$ that can be evaluated

on a dataset, respectively. Hence, without possible confusion, when evaluating we can use $\widehat{S}f$ and $\widehat{S}'f'$ even when $f \notin \mathcal{H}_w$ or $f' \notin \mathcal{H}'_w$.

Now, as shown in [26], the empirical estimator $\widehat{\mathcal{T}}_w$ of the transfer operator \mathcal{T} using dataset \mathcal{D}_n can be obtained via operator regression by minimizing the empirical risk

$$\|\widehat{S}' - \widehat{S}\widehat{\mathcal{T}}_w\|_{\text{HS}}^2 = \|\widehat{S}' - \widehat{S}E_w\widehat{\mathcal{T}}(E'_w)^*\|_{\text{HS}}^2 = \|\widehat{S}'E'_w - \widehat{S}E_w\widehat{\mathcal{T}}\|_{\text{HS}}^2$$

where the last equality holds since E'_w is a partial isometry. Therefore, the simple least square (LS) estimator is than obtained as $\widehat{\mathcal{T}} := (E_w^* \widehat{S}^* \widehat{S}E_w)^\dagger (E_w^* \widehat{S}^* \widehat{S}'E'_w) = (\widehat{C}_X^w)^\dagger \widehat{C}_{XX'}^w$, or, equivalently, as $\widehat{\mathcal{T}}_w = E_w\widehat{\mathcal{T}}(E'_w)^* = \widehat{S}^*(\widehat{S}\widehat{S}^*)^\dagger \widehat{S}'$

Once the regression is performed, recalling that X' is a $\Delta t = 1$ step ahead evolution of X we can use it to approximate $\mathbb{E}[f(X') | X = x] \approx (\widehat{\mathcal{T}}_w f)(x)$ for $f: \mathcal{X} \rightarrow \mathbb{R}$, as the following result shows.

Proposition 3. *Let $\widehat{\mathcal{T}}: \mathcal{H}'_w \rightarrow \mathcal{H}_w$ be a LS estimator of \mathcal{T} , then for every $x \in \mathcal{X}$ and $f \in \mathcal{H}_w$*

$$(\widehat{\mathcal{T}}_w f)(x) = \psi_w(x)^\top (\widehat{C}_X^w)^\dagger \widehat{\Psi}_X[f(x'_1) | \dots | f(x'_n)]^\top, \quad (40)$$

where $\widehat{\Psi}_X := [\psi_w(x_1) | \dots | \psi_w(x_n)] \in \mathbb{R}^{r \times n}$.

Proof. The proof follows directly observing that $\widehat{\Psi}_X^\top = \sqrt{n}[\widehat{S}\psi_{w,1} | \dots | \widehat{S}\psi_{w,r}] = \sqrt{n}\widehat{S}E_w$. Namely, then

$$\widehat{\Psi}_X[f(x'_1) | \dots | f(x'_n)]^\top = (\widehat{S}E_w)^* \widehat{S}'f = E_w^* \widehat{S}^* \widehat{S}'f = E_w^* \widehat{S}^* \widehat{S}'E_w E_w^* f = \widehat{C}_{XX'}^w E_w^* f$$

and, hence

$$\psi_w(x)^\top (\widehat{C}_X^w)^\dagger \widehat{\Psi}_X[f(x'_1) | \dots | f(x'_n)]^\top = E_w(\widehat{C}_X^w)^\dagger \widehat{C}_{XX'}^w E_w^* f = \widehat{\mathcal{T}}_w f.$$

□

We remark that the previous result formally holds for $f \in \mathcal{H}'_w$, but it can be easily extended to functions in $L^2_{\mu'}(\mathcal{X})$ via interpolation.

D.3 Dynamics mode decomposition and forecasting

Now we consider the problem of forecasting the process for several time steps in future using what is known as (extended) dynamic mode decomposition, which is based on the estimated eigenvalues and eigenfunctions of the transfer operator. As observed in the main body, this is meaningful only if the operator is an endomorphism on a function space, i.e. if it maps the space into itself.

Hence, after training DPNet we will use just one representation ψ_w and its r -dimensional space of functions $\mathcal{H}_w := \text{span}(\psi_{w,j})_{j \in [r]}$ to perform the operator regression, as explained in the previous section, and obtain an estimator $\widehat{\mathcal{T}}_w = E_w\widehat{\mathcal{T}}E_w^*: \mathcal{H}_w \rightarrow \mathcal{H}_w$, for some matrix $\widehat{\mathcal{T}} \in \mathbb{R}^{r \times r}$. Then, if $(\widehat{\lambda}_i, \widehat{u}_i, \widehat{v}_i)_{i \in [r]} \subset \mathbb{C} \times \mathbb{C}^r \times \mathbb{C}^r$ is a spectral decomposition of $\widehat{\mathcal{T}}$, then $(\widehat{\lambda}_i, E_w\widehat{u}_i, E_w\widehat{v}_i)_{i \in [r]}$ is a spectral decomposition of $\widehat{\mathcal{T}}_w$. In the following result we show how to compute dynamic mode decomposition of \mathcal{T} based on the estimator $\widehat{\mathcal{T}}_w$ and use it for forecasting by approximating $\mathbb{E}[f(X_t) | X_0 = x] \approx ((\widehat{\mathcal{T}}_w)^t f)(x)$, for $f: \mathcal{X} \rightarrow \mathbb{R}$, $x \in \mathcal{X}$.

Proposition 4. *Let $\widehat{\mathcal{T}}_w = E_w\widehat{\mathcal{T}}E_w^*: \mathcal{H}_w \rightarrow \mathcal{H}_w$ be rank r LS estimator of $\mathcal{T}_{\Delta t}$, for $\Delta t = 1$. If $\widehat{\mathcal{T}} = \sum_{i \in [r]} \widehat{\lambda}_i \widehat{v}_i \widehat{u}_i^*$ is the spectral decomposition of $\widehat{\mathcal{T}}$, and $\widehat{g}_i(x) := \psi_w(x)^\top \widehat{v}_i$ and $\widehat{f}_i(x) := (\widehat{u}_i)^* \psi_w(x)$, $i \in [r]$, then for every $t \in \mathbb{N}$, every $x \in \mathcal{X}$ and every $f \in \mathcal{H}_w$ it holds that*

$$((\widehat{\mathcal{T}}_w)^t f)(x) = \sum_{i \in [r]} \widehat{\lambda}_i^t \widehat{g}_i(x) \widehat{u}_i^* D_w(f), \quad (41)$$

where $D_w(f) := \widehat{\Lambda}^{-1}(\widehat{C}_X^w)^\dagger \widehat{\Psi}_X[f(x'_1) | \dots | f(x'_n)]^\top \in \mathbb{R}^r$.

Proof. First observe that

$$(\widehat{\mathcal{T}}_w)^t f = E_w\widehat{\mathcal{T}}^t E_w^* f = E_w\widehat{\mathcal{T}}^{t-1} E_w^* E_w\widehat{\mathcal{T}} E_w^* f = \sum_{i \in [r]} \widehat{\lambda}_i^{t-1} (\widehat{g}_i \otimes \widehat{f}_i) E_w\widehat{\mathcal{T}} E_w^* f.$$

Hence,

$$((\widehat{\mathcal{T}}_w)^t f)(x) = \sum_{i \in [r]} \widehat{\lambda}_i^{t-1} \widehat{g}_i(x) (\widehat{u}_i^* \widehat{\mathcal{T}} E_w^* f) = \sum_{i \in [r]} \widehat{\lambda}_i^t \widehat{g}_i(x) (\widehat{\lambda}^{-1} \widehat{u}_i^* \widehat{\mathcal{T}} E_w^* f)$$

and the rest of the proof follows as in Prop. 3. □

We remark that $\widehat{u}_i^* D_w(f)$ is known as i -th Koopman mode of the observable f , and that in comparison to Encoder-Decoder approaches $D_w(f)$ can be considered as a decoder when forecasting function $f: \mathcal{X} \rightarrow \mathbb{R}$. Clearly this is easily extended to vector valued functions, and, hence, we can forecast the states by using $\widehat{u}_i^* D_w(I) := \widehat{\Lambda}^{-1}(\widehat{C}_X^w)^\dagger \widehat{\Psi}_X[x'_1 | \dots | x'_n]^\top \in \mathbb{R}^d$, where $\mathcal{X} \subset \mathbb{R}^d$.

E SDE learning

We first prove the main result of Sec. 5. Recalling (20), we have introduced the score for training continuous-time DPNets via the partial trace w.r.t. a subspace. Hence, we first show the following auxiliary result.

Lemma 3. *Let \mathcal{H} be a separable Hilbert space and let $\mathcal{H}_r \subseteq \mathcal{H}$ be a (finite) r -dimensional subspace. If $A: \mathcal{H} \rightarrow \mathcal{H}$ is a self-adjoint operator having at least $r + 1$ eigenvalues $\lambda_1(A) \geq \lambda_2(A) \geq \dots \geq \lambda_r(A) \geq \lambda_{r+1}(A)$ above its essential spectrum, then*

$$\text{tr}(AP_{\mathcal{H}_r}) \leq \lambda_1(A) + \lambda_2(A) + \dots + \lambda_r(A),$$

and equality holds when \mathcal{H}_r is spanned by eigenfunctions of A corresponding to eigenvalues $\lambda_1(A), \dots, \lambda_r(A)$.

Proof. First, let $(v_i)_{i \in [r]}$ denote eigenvectors of A corresponding to eigenvalues λ_i , i.e. $Av_i = \lambda_i(A)v_i$, and let $(h_i)_{i \in \mathbb{N}}$ be an ortho-normal basis of \mathcal{H} such that $(h_i)_{i \in [r]}$ is the ortho-normal basis of \mathcal{H}_r . Then, clearly

$$\text{tr}(AP_{\mathcal{H}_r}) = \text{tr}(P_{\mathcal{H}_r}AP_{\mathcal{H}_r}) = \sum_{i \in \mathbb{N}} \langle h_i, (P_{\mathcal{H}_r}AP_{\mathcal{H}_r})h_i \rangle = \sum_{i \in [r]} \langle h_i, Ah_i \rangle, \quad (42)$$

which is clearly equal to $\lambda_1(A) + \lambda_2(A) + \dots + \lambda_r(A)$ whenever $h_i = v_i$, $i \in [r]$.

The upper bound we prove by induction. First, for $r = 1$ we have that $\langle h_i, Ah_i \rangle \leq \lambda_1(A)$ follows directly from the Courant-Fischer max-min theorem for operators which claims that

$$\lambda_i(A) = \max_{h_1, \dots, h_i} \min\{\langle h, Ah \rangle \mid h \in \text{span}(h_j)_{j \in [i]}, \|h\| = 1\}, \quad i \in [r+1]$$

Next, assuming that (42) holds for arbitrary A and $r \leq m - 1$, we will prove that it holds for $r = m$.

Start by observing that there exists $\mathcal{H}' \subseteq \mathcal{H}_m$ such that $\dim(\mathcal{H}') \leq m - 1$ and $\mathcal{H}' \perp v_1$. Indeed, taking $g_i = \sum_{j \in [m]} b_{ij}h_j$, $i \in [m - 1]$, for some $B = [b_{ij}] \in \mathbb{R}^{(m-1) \times m}$, we have that $g_i \perp v_1$ for all $i \in [m - 1]$ iff $B\beta = 0$, where the vector $\beta \in \mathbb{R}^m$ is given by $\beta_j = \langle h_j, v_1 \rangle$. Now, if $\beta = 0$, then $\mathcal{H}_m \perp v_1$ and the claim trivially follows. Otherwise, since $\dim(\text{span}(\beta)^\perp) = m - 1$, there exists a matrix $B \in \mathbb{R}^{(m-1) \times m}$ so that $B\beta = 0$. Consequently, the space \mathcal{H}' spanned by $(g_i)_{i \in [m-1]}$ is such that $\dim(\mathcal{H}') \leq m - 1$ and $\mathcal{H}' \subseteq \text{span}(v_1)^\perp$. Without the loss of generality, assume that $(g_i)_{i \in [m-1]}$ are orthonormal basis of \mathcal{H}' and that g_m is such that $(g_i)_{i \in [m]}$ are orthonormal basis of \mathcal{H} .

First, clearly $\langle g_m, Ag_m \rangle \leq \lambda_1$. On the other hand, define $A' := A + (\lambda_{r+1} - \lambda_1)v_1 \otimes v_1$. This is an operator obtained by deflating (moving) the first eigenvalue into the $(r + 1)$ -th one. Namely, we have that $\lambda_i(A') = \lambda_{i+1}(A)$ for $i \in [m - 1]$. Moreover, it holds that $A'P_{\mathcal{H}'} = AP_{\mathcal{H}'}$. Hence, according to the inductive hypothesis, we have

$$\text{tr}(AP_{\mathcal{H}'}) = \text{tr}(A'P_{\mathcal{H}'}) \leq \sum_{i \in [m-1]} \lambda_i(A') = \sum_{i=2}^m \lambda_i(A),$$

and, consequently,

$$\text{tr}(AP_{\mathcal{H}}) = \sum_{i \in [r]} \langle g_i, Ag_i \rangle = \text{tr}(AP_{\mathcal{H}'}) + \langle g_m, Ag_m \rangle \leq \sum_{i=2}^m \lambda_i(A) + \lambda_1(A) = \sum_{i \in [m]} \lambda_i(A),$$

which completes the proof. \square

Theorem 2. *If $\mathcal{H}_w \subseteq L_\pi^2(\mathcal{X})$ and \mathcal{L} has at least $r + 1$ eigenvalues above its essential spectrum, then*

$$\mathcal{P}_\partial(w) = \text{tr}((C_X^w)^\dagger C_{X\partial}^w) \leq \lambda_1(\mathcal{L}) + \dots + \lambda_r(\mathcal{L}), \quad (23)$$

where $\lambda_1(\mathcal{L}) \geq \lambda_2(\mathcal{L}) \geq \dots$ are eigenvalues of \mathcal{L} . Moreover, if for every $j \in [r]$ function $\psi_{w,j}$ is the eigenfunction of \mathcal{L} corresponding to eigenvalue $\lambda_j(\mathcal{L})$, then equality in (23) holds.

Proof. In view of Lem. 3, we only need to prove that $\text{tr}(P_{\mathcal{H}_w} \mathcal{L} P_{\mathcal{H}_w}) = \text{tr}((C_X^w)^\dagger C_{X\partial}^w)$. To that end, we reason as in the proof of Lem. 2 to obtain that $P_{\mathcal{H}_w} = UQ(C_X^w)^{\dagger/2} Q^* S_\pi^*$, where $S_\pi: \mathcal{H}_w \hookrightarrow L_\pi^2(\mathcal{X})$ is an injection and $Q: \mathbb{R}^r \rightarrow \mathcal{H}_w$ and $U: \mathcal{H}_w \rightarrow L_\pi^2(\mathcal{X})$ are partial isometries. Moreover, recalling (19), we have that

$$\begin{aligned} (Q^* S_\pi^* \mathcal{L} S_\pi Q) &= \lim_{\Delta t \rightarrow 0^+} \frac{Q^* S_\pi^* (\mathcal{T}_{\Delta t} - I) S_\pi Q}{\Delta t} \\ &= \lim_{\Delta t \rightarrow 0^+} Q^* \left[\int_{\mathcal{X}} \pi(dx) \phi_X^w(x) \otimes \frac{\int_{\mathcal{X}} p_{\Delta t}(x, dx') (Q^* \phi_X^w(x') - Q^* \phi_X^w(x))}{\Delta t} \right] \\ &= \int_{\mathcal{X}} \pi(dx) \psi_w(x) \otimes \left(\lim_{\Delta t \rightarrow 0^+} \frac{\int_{\mathcal{X}} p_{\Delta t}(x, dx') (\psi_w(x') - \psi_w(x))}{\Delta t} \right) \\ &= \mathbb{E}_{X \sim \pi} [\psi_w(X) \otimes d\psi_w(X)] = C_{X\partial}^w, \end{aligned}$$

where the last line follows from Itô formula (see e.g. [4]). Hence, using $P_{\mathcal{H}_w} = UQ(C_X^w)^{\dagger/2} Q^* S_\pi^*$ we have that

$$\text{tr}(P_{\mathcal{H}_w} \mathcal{L} P_{\mathcal{H}_w}) = \text{tr}((C_X^w)^{\dagger/2} C_{X\partial}^w (C_X^w)^{\dagger/2}) = \text{tr}((C_X^w)^\dagger C_{X\partial}^w),$$

which completes the proof \square

To conclude this section, we remark that in the continuous setting the estimator $\widehat{\mathcal{L}}_w: \mathcal{H}_w \rightarrow \mathcal{H}_w$ of \mathcal{L} on the learned space \mathcal{H}_w can be obtained via operator regression in a similar way as discussed in Sec. 4. So, the LS estimator is given by matrix $\widehat{L} = (\widehat{C}_X^w)^\dagger \widehat{C}_{X\partial}^w$, and its spectral decomposition is

$$\widehat{\mathcal{L}}_w = \sum_{i \in [r]} \widehat{\lambda}_i \widehat{g}_i \otimes \widehat{f}_i, \quad \text{where} \quad \widehat{g}_i(x) := \psi_w(x)^\top \widehat{v}_i \quad \text{and} \quad \widehat{f}_i(x) := (\widehat{u}_i)^* \psi_w(x), \quad (43)$$

where $\widehat{L} = \sum_{i \in [r]} \widehat{\lambda}_i \widehat{v}_i \widehat{u}_i^\top$ is the spectral decomposition of the matrix \widehat{L} .

Hence, using that $\lambda_i(\mathcal{T}_{\Delta t}) = \exp(\lambda_i(\mathcal{L}))$, we directly obtain the modal decomposition in the continuous time,

$$\mathbb{E}[f(X_t) | X_0 = x] \approx \sum_{i \in [r]} \exp(\widehat{\lambda}_i t) \widehat{g}_i(x) \widehat{u}_i^* D_w(f), \quad t \in [0, +\infty) \quad (44)$$

where $D_w(f) = (\widehat{C}_X^w)^\dagger \widehat{\Psi}_X [f(x_1) | \dots | f(x_n)]^\top \in \mathbb{R}^r$ are the coefficients of the LS estimator of f in \mathcal{H}_w . As a final remark, note that in (44) we regress function f onto \mathcal{H}_w using least squares with data $(x_i, f(x_i))$.

F Experiments

The code to reproduce the experiments can be found at the url <https://anonymous.4open.science/r/DPNets-FE37>. Except for the pendulum experiment (discussed below), the experiments were performed on a workstation equipped with an Intel(R) Core™ i9-9900X CPU @ 3.50GHz, 48GB of RAM and a NVIDIA GeForce RTX 2080 Ti GPU. We also have used PyTorch 1.13.0 for the Chignolin experiment and JAX 0.4.9 for the others.

F.1 Pendulum

Setup. We considered the 2-dimensional dynamical system representing the position and velocity of a pendulum, which is modeled by the second order differential equation $\ddot{\theta} + (g/\ell) \sin \theta = 0$, with $l = 1$, $g = 9.8$ being the length of the pendulum and gravity respectively. This system is deterministic and with continuous spectra (see e.g. [34]), but our method can still be applied (see also Remark 1). We replicate exactly the setup of [6]⁴. In particular, the dataset is constructed by sampling a single trajectory of 1700 points (600 of which are used for training and the rest for validation) from the initial angles $\theta_0 = 2.4$ and $\dot{\theta}_0 = 0.8$ with zero initial velocity. We finally apply a linear map to the 2 dimensional state to get a high-dimensional state of dimension 64 which is used for learning. Each element of the matrix representing this linear map is sampled from a Gaussian distribution.

Network Architecture. We use the network architecture described in [6], where the parameter α tunes the width. The encoder network has 3 feed-forward layers with tanh activation on the first two and no activation in the last (output) layer. The hidden dimension of the first two is $16 \times \alpha$, while for the last it is equal to the “bottleneck” parameter. The decoder network has the same structure but the input dimension of the first layer and the output dimension of the last are swapped and tanh is applied also to the last layer. For CAE we use both encoder and decoder networks, while the other methods use only the encoder since the linear decoder map is computed after training.

⁴We follow the code at <https://github.com/erichson/koopmanAE>

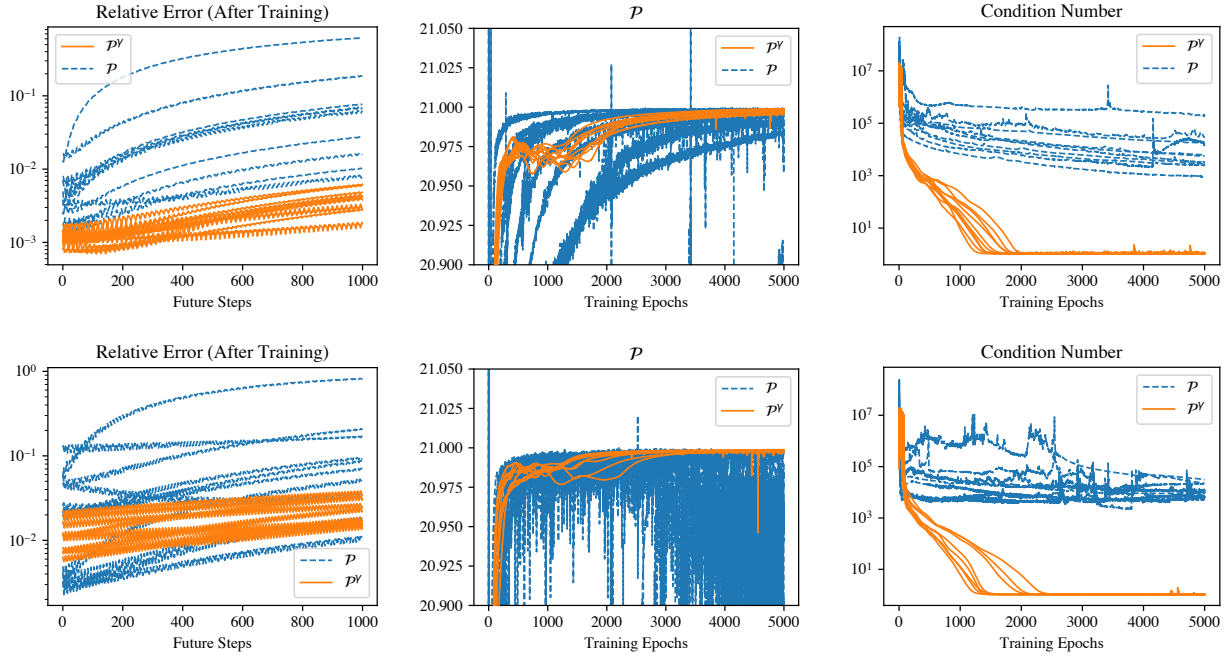


Figure 4: Relative error on the validation set (left), \mathcal{P} computed on the training set (center), and condition number of the training input covariance (right) for 10 different runs (varying only network initialization). Each line for the relative error is averaged over 30 starting points. First row shows the results for $\theta_0 = 2.4$ while second row for $\theta_0 = 0.8$. The optimal value for \mathcal{P} is 21, since the pendulum has unitary transition operator and we learn 21 features. Each epoch corresponds to a step of the optimizer.

Hyperparameters. For CAE, we keep the same hyperparameters used in the implementation provided by [6], which match the one reported in the paper. In particular, we set $\alpha = 1$, $\lambda = 1$, $\nu = 0.01$, $\eta = 0.002$, the bottleneck to 6, the batch size to 64, the starting learning rate to 0.01 (multiplied by 0.2 at epochs $\{30, 200, 400, 500\}$), gradient clipping to 0.05, the number of forward and backwards steps to 8 and we train for 600 epochs with the AdamW optimizer. We note that the results reported in Table 1 are comparable to the ones in [6, Table 1 row 2, 6]. For \mathcal{P} and \mathcal{P}^γ we choose hyperparameters by hand with a few trials. In particular, we set $\alpha = 2$, $\gamma = 1$ for \mathcal{P}^γ then we set the bottleneck (number of learned features) to 21, the learning rate to 0.05 for \mathcal{P} and 0.005 for \mathcal{P}^γ , and we train for 5000 epochs with the AdamW optimizer. We use the entire dataset of 600 points at each iteration (full batch training). The total number of network parameters for CAE is 2958 while for $\widehat{\mathcal{P}}$ and $\widehat{\mathcal{P}}^\gamma$ is 3796.

The effect of orthonormality regularization. We additionally perform a comparison between \mathcal{P} and \mathcal{P}^γ where we select, for each (method, θ_0) pair, the learning rate which maximises \mathcal{P} (the average over 10 runs) computed on the training set after 5000 epochs. We choose the learning rate among the ten values $\{0.0001, 0.0005, 0.001, 0.005 \dots 1, 5\}$. According to this procedure, the best learning rate for \mathcal{P}^γ is 0.005 regardless of θ_0 , while for $(\mathcal{P}, \theta_0 = 0.8)$ and $(\mathcal{P}, \theta_0 = 2.4)$ the best learning rates are 0.1 and 0.05 respectively. The other parameters are kept the same as in the previous experiment except that we set $\gamma = 0.1$ for \mathcal{P}^γ . In Figure 4 we report results for 10 training runs with the chosen learning rates, where only the initialization of the neural network changes. We observe that despite the limited amount of randomness (full batch training and same dataset across runs) the Relative error and \mathcal{P} vary greatly among runs when optimizing only \mathcal{P} without orthonormality regularization, while optimizing \mathcal{P}^γ yields smoother and more consistent plot lines. Furthermore, when optimizing only \mathcal{P} , \mathcal{P} sometimes spikes above its maximum allowed value of 21, indicating that its computation is unstable due to the high condition number of the training covariance (right plot). On the contrary, with the addition of the regularization term, the condition number is generally lower throughout training and always converges near one, thus making the computation of \mathcal{P} more reliable.

Relevant implementation details. Computing \mathcal{P} requires to compute the square-root pseudo-inverse of the input and output empirical covariance matrices. To do it we follow the implementation in [23], where we first compute the eigenvalue decomposition (via `torch.linalg.eigh`⁵) of the Tikhonov-regularized input and output covariance matrices with

⁵We use PyTorch 2.0.0 with CUDA 11.7.

regularization parameter set to 10^{-6} and then we compute the inverse square-root of the eigenvalues. All experiments in Table 1 were run on the GPU. However, we found that the GPU implementation performs significantly worse than the CPU one for the \mathcal{P} method. We suspect this to be due to the more efficient but less accurate GPU implementation of `torch.linalg.eigh`. Due to of this, we observed qualitatively similar plots to the ones in Figure 4 also when training on the CPU, but only when we learn a higher number of features (we tried with 31).

Hardware Used. We executed the pendulum experiments on an Alienware Desktop from 2018 having an i9 Intel CPU with 12 cores and 24 threads and 2 NVIDIA GTX 1080 Ti GPUs with 11 GB of memory, only one of which is used for each run.

F.2 Fluid dynamics

The data for this experiment are equally spaced sampled solutions of the Navier-Stokes equations [49] for an incompressible Newtonian fluid coupled with the transport equation

$$\partial_t c + \mathbf{u} \cdot \nabla c = \text{Pec}^{-1} \nabla^2 c.$$

Here, Pec is the Péclet number, and $c : \mathbb{R}^3 \rightarrow \mathbb{R}$ is a field representing the concentration $c(t; x, y)$ of a scalar quantity which is transported by the fluid flow without influencing the fluid motion itself (e.g. a dye dissolved in water). These partial derivative equations are solved over a 100×200 regular grid.

In the main text we reported not having been able to successfully train DPNets on this dataset using \mathcal{P}^γ as a score function. Indeed, we tried different combinations of optimizer (SGD, Adam and AdamW), learning rates ($10^{-5}, 5 \times 10^{-5}, 10^{-4}, 5 \times 10^{-4}, 10^{-3}, 5 \times 10^{-3}, 10^{-2}$) and regularization strength γ ($0, 10^{-5}, 10^{-4}, 10^{-3}, 10^{-2}, 10^{-1}, 1$) for a total of 147 combinations. Out of them only 73 reached the threshold of 5000 iterations, while the others crashed due to exploding gradients or linear algebra errors. Out of the 74 finished runs, however, only 6 of them are such that the condition number of the covariance matrix is smaller than 10^5 . As argued on the main text, indeed, a large condition number makes unreliable even the *evaluation* of \mathcal{P} . The remaining 6 candidates result in values of the \mathcal{P} score (the largest of which is $\mathcal{P} = 19$, condition number 1.02) worse than what obtained ($\mathcal{P} = 25.8$, condition number 1.781) by optimizing over \mathcal{S} with the same computational budget. The parameters used to produce the plots showed in the main text are as follows.

Data. Available at <https://github.com/maziarraissi/HFM>. It consists of 201 snapshots: 160 used for training, the rest for testing. Has been standardized: each channel with its own mean and std.

Optimization. Adam with learning rate 10^{-4} . Other parameters are the predefined values in Optax’s implementation. No mini-batching. 5000 total training iterations/epochs. The training time is ≈ 39 mins.

Architecture. $3 \times [\text{Conv2d} \rightarrow \text{ReLU} \rightarrow \text{AvgPool}] \rightarrow \text{Flatten} \rightarrow \text{Dense}[256] \rightarrow \text{Dense}[32]$

Hyperparameters. Orthogonality regularization $\gamma = 5$; Chapman-Kolmogorov regularization (when used) $\eta = 50$.

F.3 Continuous dynamics

The implementation of this experiment is straightforward, and our results can be reproduced using the following informations.

Data. Produced in-house with JAX MD. Both the dataset and the script to produce new trajectories will be released. The dataset consists of 10^5 snapshots: 70% used for training, 10% for validation, 20% for testing.

Optimization. Adam with learning rate 10^{-3} . Other parameters are the predefined values in Optax’s implementation. Batch size: 8192. 500 epochs. Training time is ≈ 2 mins.

Architecture. Multi layer perceptron with CeLu activation function. Dimension of the hidden layer: [32, 64, 128, 128, 64, 4].

Hyperparameters: Orthogonality regularization $\gamma = 50$.

F.4 The metastable states of Chignolin

This is by far the heaviest experiment of the paper, and we made use of the package SchNetPack [44, 45] on multiple instances. In particular, we have used SchNetPack dataloaders and preprocessing transformations (casting to 32 bit precision and on-the fly computation of the distance matrix). Further, we have used SchNetPack’s implementation of the SchNet interaction block. To reproduce our results, the following informations may prove useful.

Data. The data was presented for the first time in [33] and is freely available for non-commercial use upon request to DeShaw research. Dataset of 524743 snapshots. Each graph is composed by the 93 heavy atoms. The edges are formed only if two atoms are less than 5 Angstroms distant. The average number of edges is 28.

Optimization. Adam with learning rate 10^{-3} . Other parameters are the predefined values in Torch's implementation. Batch size: 192. 100 epochs. Training time: ≈ 11 hrs.

Architecture. SchNet with 3 blocks, 20 RBF functions expansions, 64 latent dimension. At the output of SchNet, the hidden variables associated to the nodes are averaged and forwarded to a dense layer with 16 final output features.

Hyperparameters. Orthogonality regularization $\gamma = 0.01$.